AO-154Y

An Integration
of

Landsat and Geophysical Data

North Eastern Arizona

Prepared for

United States Geological Survey

by

S.I. Gutman
G.A. Heckmann

AN INTEGRATION OF LANDSAT AND GEOPHYSICAL DATA IN NORTHEASTERN ARIZONA

by

Seth I. Gutman and Gary A. Heckmann

GS Laboratories
1210 North Lyon Street
Santa Ana, California 92701

A Report of Work Performed Under
USGS Contract Number 94599

for

The United States Geological Survey
Reston, Virginia 22092

October, 1977

TABLE OF CONTENTS

LIST OF FIGURES

LIST OF PLATES

LIST OF TABLES

ABSTRACT

ABSTRACT

A one year study was undertaken on behalf of the U. S. Geological Survey to examine the ways in whicn LANDSAT data integrates with selected geophysical methods in northeastern Arizona. The purpose of this paper is to summarize the results obtained from this study.

LANDSAT imagery with partial snow cover and a low sun angle was acquired to enhance structural features. A final structural interpretation was performed on 1:500,000 scale images.

Residual magnetic intensity data derived from Sauck and Sumner's aeromagnetic survey of Arizona were continued to a common flight line elevation and contoured. This map, along with other magnetic data, were interpreted to define the configuration of the magnetic basement and to identify significant tectonic features in the study area.

Bouguer gravity anomaly data, derived from several sources, were used to create and interpret a residual Bouguer anomaly map of northeastern Arizona.

The results were then integrated so as to achieve an internally consistent final interpretation.

This interpretation is analyzed in the light of the regional geophysics and geology; its implications are examined with respect to the geology of the Colorado Plateau and the oil and gas, geothermal and mineral potential of the study area.

1.0 INTRODUCTION

1.0 Introduction

The purpose of this study is to examine the ways in which information derived from LANDSAT Multispectral imagery integrates with other geophysical methods such as gravity and magnetics to achieve an internally consistent final interpretation of the data.

When we refer to this as an integrated study we mean that the utilization of LANDSAT imagery, along with geophysical data, results in a more complete, harmonious or coordinated final interpretation than would otherwise be possible.

The structural interpretation of LANDSAT imagery is often a highly subjective procedure; the results are (commonly) very sensitive to the experience of the geoscientist and the quality of his data. None-the-less, it has been shown by almost all serious users of orbital remote sensing data, that valuable information can be derived from them if careful attention to the geologic implications and plausibilities of the interpreted features is paid.

While the quantitative interpretation of potential field data has been adequately discussed in the literature for almost three decades and the advent of high speed computers

has made the detailed analysis of large quantities of potential field anomalies routine, the direct structural interpretations of potential field maps remains a highly subjective affair. This is perhaps even more true of magnetic data than gravity data because the involved interactions of the strike and dip, shape and magnetization characteristics of the anomaly-causing bodies with the local inclination and declination of the earth's magnetic field. For example, while it is common to observe a high gradient associated with the scarp of a faulted block in gravity data, this is true in magnetics only when: the level of the survey is close to the anomaly causing body; the body is much longer than it is wide and strikes (generally) magentic east-west; or, when the data has been reduced to the pole (transformation of the inclined field to vertical). It is clear that these are rare occurrences or, in the case of the last condition, require a mathematical manipulation of the data which could introduce unforeseen errors and bogus information into the map.

The interpreted configuration of the Precambrian basement in the study area was derived from a quantitative analysis of selected magnetic anomalies and the combined examination of Bouguer anomaly and residual magnetic intensity maps (Plates 4 and 5). The contribution of the LANDSAT data to this procedure was nil, providing only confidence that the

interpreted structural pattern (which in many cases is orthogonal to that defined by the surface mapping), has an observable surface manifestation.

The authors take full responsibility for the contents and conclusions of this report and any inaccuracies that occur herein. Apologies are made to any individuals not appropriately credited for their contributions to this study. We wish to especially acknowledge the following individuals who have made a direct contribution to the study: W. A. Fischer, J. Walden and J. Denoyer of the U. S. Geological Survey EROS Program; M. A. Liggett of Cyprus Georesearch Company; J. N. Conley of the State of Arizona Oil and Gas Conservation Commission; J. S. Sumner of the University of Arizona; C. Underwood, B. Dickman and R. Russel of Information Systems Design Inc., Santa Clara California; and K. McClanahan for clerical and drafting support.

Santa Ana, California
January, 1978

S. I. Gutman,
G. A. Heckmann,

2.0 REVIEW OF TECTONICS AND STRUCTURAL GEOLOGY

2.1 Review of Tectonics and Structural Geology.

The tectonic elements and structural geology of the Colorado Plateau have been discussed in great detail by many authors (Kelley and Clinton, 1960; Kelley, 1955a; Kelley, 1955b; Kelley, 1958; Hodgson, 1968; Hodgson, 1965; Davis, 1975; Woodward, 1973) and a critical analysis of these works is beyond the scope of the report. A few points, salient to the work to be presented in subsequent sections are presented:

- Jointing and fracture systems vary in character, persistency, frequency, orientation and age between not only the various tectonic elements of the Plateau but even within a single element (Kelley and Vincent, 1960).
- Maximum deformation occurs in long narrow zones (monoclinal flexures) which commonly mark the boundaries of tectonic elements (Davis, 1975).
- The structural grain (Hodgson's "fracture trends"), in the Precambrian basement (of the Grand Canyon region) is present in the overlying sedimentary rocks (Hodgson, 1965).
- In the Study area, fold axes trend predominantly north-northeast to northeast. Old Precambrian folding is generally northeast-southwest, while younger (Laramide age) deformation is characteristically northwest-southeast and north-south (Wilson, 1962).

Figure 3 and Plate 1 are included in this report primarily as references; they will be referred to, as required, throughout the text.

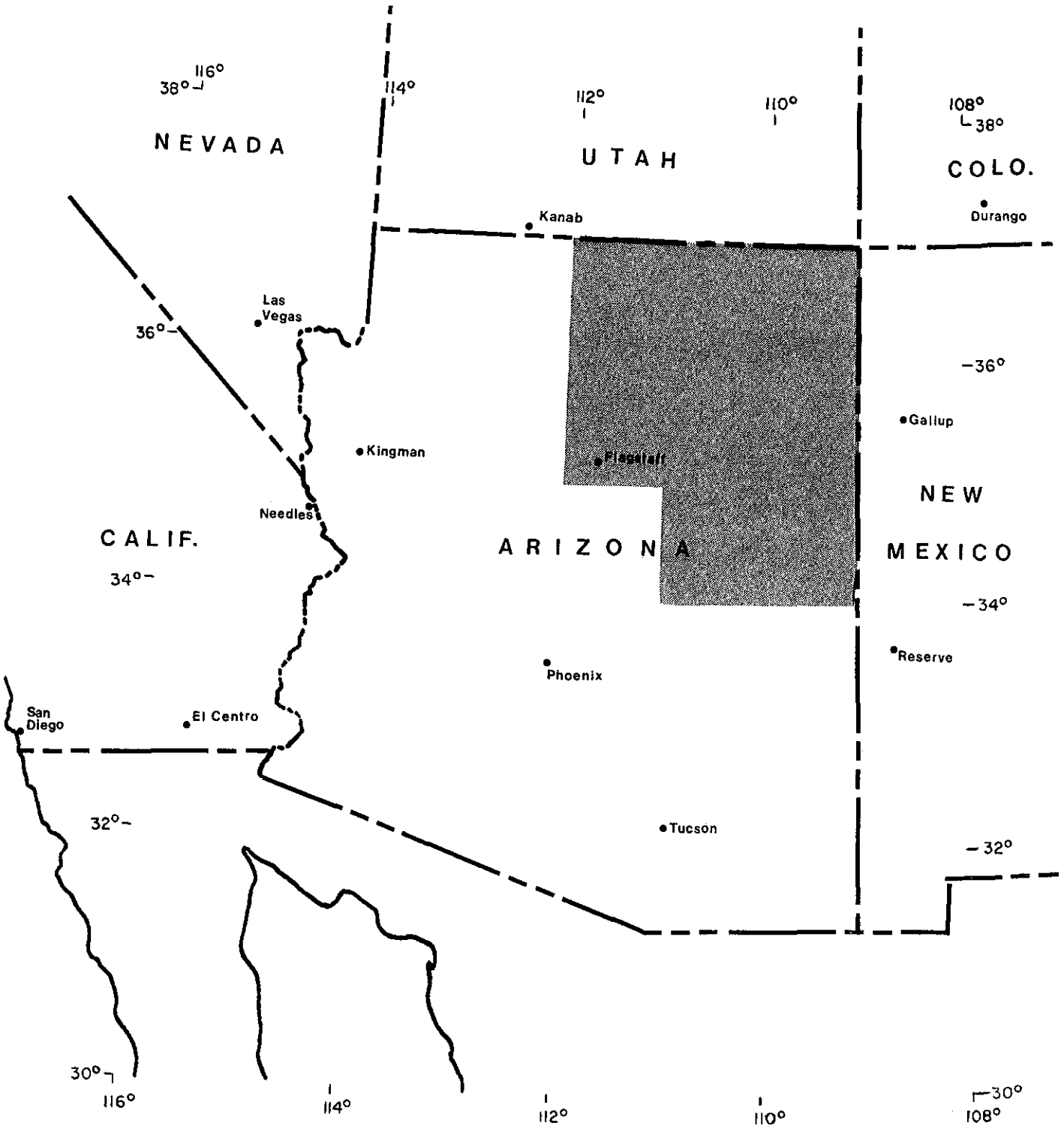

Location Map

Fig. (1)
Index map of Southwestern United States showing location of USGS study area.

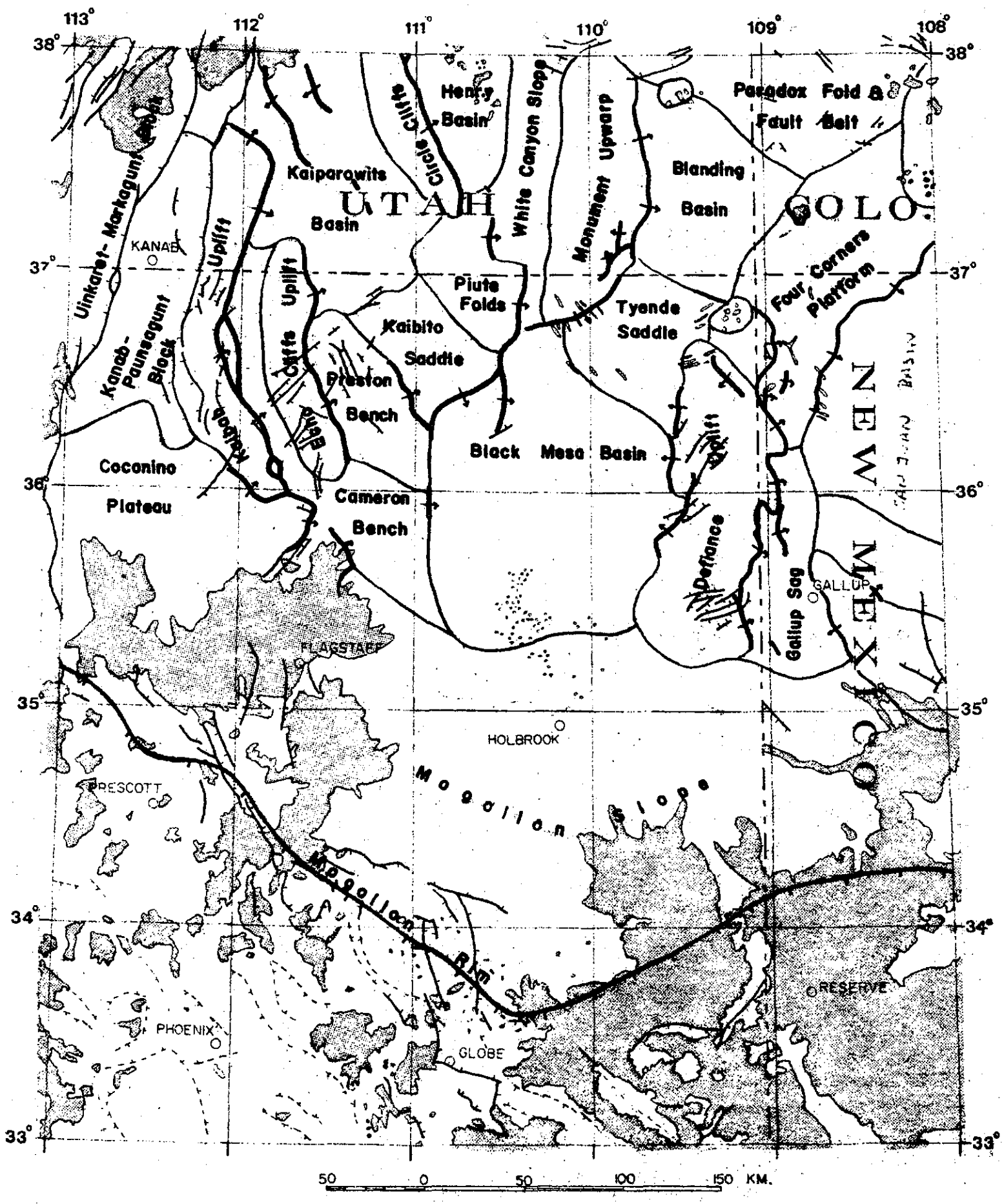

Fig. (2) Tectonic subdivisions of a portion of the Colorado Plateau

3.0 REGIONAL GEOPHYSICS

3.1 Introduction

An examination of the regional geophysical environment of the study area is presented. Seismicity, regional gravity and geothermal gradient data was evaluated to aid in the reduction of the detailed geophysical data, and provide inputs into the relationship of the area to the Colorado Plateau and the tectonics of the southwestern United States.

3.2.1 Seismicity

The Colorado Plateau, as defined by Kelley and others (Kelley and Clinton, 1960), is characteristically aseismic. The eastern and western boundaries of the plateau are defined by generally North-South trending faults with moderate seismic activity. Most of the activity in these regions is in the form of microseismic events (Simon, 1972). This data along with other geophysical and geological information has led Smith and Sbar (1974) to define the Intermountain Seismic Belt (ISB) which they suggest represents an intracontinental subplate boundary. The Southern extremity of the ISB is associated with the Paunsagunt fault zone which lies at the Northwest edge of the study area.

3.2.2 Seismicity Data.

Table 3.1 is derived from data supplied by the National Oceanic and Atmospheric Administration (NOAA, 1976). It includes all earthquakes of magnitude 4.0 and greater (lower where locally monitored) between the years 1960 and 1974. For an explanation of the abbreviations used in Table 3.1 refer to Section 3.2.3.

3.2.3 Explanation of Abbreviations Used in Table 3.1

Source:

PAS	Pasadena, Ca.
CGS	Coast and Geodetic Survey
USE	United States Earthquakes
NOS	National Ocean Survey
ERL	Environmental Research Laboratories
GS	U.S. Geological Survey, Denver, Co.

Date and origin time in Universal (Greenwich) Time

Authority (follows origin time):

P	Parameters of hypocenter supplied by California Institute of Technology
*	Second-order hypocenter determination by CGS/NOS/ERL/GS using incomplete or less reliable data

Table 3.1 Earthquake Data for Study Area
with magnitude 4.0 and greater (1960-1974).

AREA SEARCH FOR GUTMAN 33-38N, 108-113W 1960-1974

SOURCE	YEAR	MO	DA	HR	MN	SEC	LAT	LONG	DEPTH (KM)	MAGNITUDES- BODY	LOCAL
PAS	1962	02	15	07	12	43.0P	36.900N	112.400W	016A		4.50MLPAS
PAS	1962	02	15	09	06	45.0P	37.000N	112.900W	016A		4.40MLPAS
PAS	1962	06	05	22	29	45.0P	38.000N	112.100W	016A		4.50MLPAS
CGS	1963	06	19	08	38	47.5	37.900N	112.600W	033		
CGS	1963	09	11	11	59	41.0	33.200N	110.700W	033	4.20MB	
PAS	1963	09	30	09	17	42.0P	38.000N	111.000W	016A		4.50MLPAS
CGS	1964	01	01	16	43	08.0	37.700N	112.500W	015		
CGS	1965	06	07	14	28	01.3	36.100N	112.200W	033		
CGS	1965	07	20	14	49	28.8	37.900N	112.500W	033		
CGS	1965	11	07	16	29	43.8	37.100N	112.400W	001		
CGS	1966	03	24	20	10	59.3	36.800N	108.300W	005		
CGS	1966	05	20	12	11	37.8	38.000N	112.100W	018		
CGS	1966	05	20	13	40	23.3	37.900N	112.100W	018		
CGS	1966	05	20	13	40	48.8	37.900N	112.100W	018	4.30MB	
CGS	1966	05	20	13	50	33.2	38.000N	112.100W	018		
CGS	1966	05	20	14	19	35.1	37.900N	112.100W	018		
CGS	1966	05	30	22	20	40.8	37.800N	112.100W	018		
CGS	1966	09	03	07	53	20.2	36.500N	112.300W	033		
CGS	1966	09	09	17	43	58.4	36.700N	108.300W	033		
CGS	1966	10	03	16	03	50.9	35.800N	111.600W	034		
CGS	1967	02	12	10	11	52.4	37.673N	108.002W	005G		
CGS	1967	03	02	06	29	24.4	34.475N	110.964W	014	3.90MB	
CGS	1967	03	28	03	48	59.1*	35.453N	111.732W	005G		
CGS	1967	05	01	19	48	07.1	34.457N	112.864W	026	3.80MB	
CGS	1967	05	08	19	31	28.5*	37.726N	110.238W	033N		
CGS	1967	05	21	18	00	05.1	34.291N	110.565W	009	3.80MB	
CGS	1967	07	20	13	51	10.4	36.300N	112.100W	033		
CGS	1967	08	07	16	24	49.3	36.500N	112.400W	033		
CGS	1967	08	07	16	40	32.1	36.400N	112.600W	033		
CGS	1967	09	04	23	27	44.7	36.200N	111.700W	033		
CGS	1968	03	20	15	33	07.0	37.800N	112.300W	033	3.90MB	
CGS	1968	08	03	15	21	25.1*	37.832N	112.268W	033N		
CGS	1968	09	20	20	32	17.3	38.010N	112.068W	033N	3.90MB	
CGS	1968	09	24	02	10	51.8	38.047N	112.068W	033N	4.00MB	
CGS	1968	09	24	02	23	16.5	37.966N	112.077W	033N		
CGS	1968	09	24	06	11	07.1	38.040N	112.145W	033N		
CGS	1969	02	21	12	08	37.2*	37.830N	112.967W	033N		
CGS	1969	03	19	09	52	15.4	37.778N	113.066W	033N		
CGS	1969	08	23	21	41	54.2	34.846N	108.698W	033N	3.90MB	
CGS	1969	11	12	20	11	42.7	37.765N	112.524W	033N		
USE	1969	12	25	12	49	10.1	33.400N	110.600W	015G	4.40MB	5.10MLCGS
CGS	1970	02	03	05	59	35.6*	37.918N	108.311W	033N	4.00MB	
CGS	1970	04	18	10	42	11.9	37.858N	111.645W	010G	4.40MB	
CGS	1970	05	23	22	55	22.4	38.074N	112.397W	003	4.60MB	4.90MLCGS
CGS	1970	05	23	23	59	24.5	38.038N	112.382W	006		2.70MLCGS
CGS	1970	05	24	01	54	32.7*	37.942N	112.416W	005G		2.20MLCGS

Table 3.1 (continued)

SOURCE	YEAR	MO	DA	HR	MN	SEC	LAT	LONG	DEPTH (KM)	--MAGNITUDES-- BODY	LOCAL
CGS	1970	05	24	01	56	05.9	38.060N	112.392W	006		2.50MLCGS
CGS	1970	05	24	02	09	53.4	38.011N	112.357W	005		2.80MLCGS
CGS	1970	08	03	19	24	17.8	34.318N	110.519W	000G		
NOS	1970	10	25	02	13	51.6	37.880N	112.341W	005G		2.30MLNOS
NOS	1970	11	24	16	47	56.0	36.357N	112.273W	006		3.00MLNOS
NOS	1970	12	03	03	47	24.6*	35.874N	111.906W	005G		2.80MLNOS
NOS	1971	01	24	20	37	37.1*	37.435N	112.521W	005G		2.40MLNOS
NOS	1971	03	14	18	14	12.2*	36.478N	110.437W	005G		2.20MLNOS
NOS	1971	03	27	04	39	11.7	36.762N	112.393W	005G		2.60MLNOS
NOS	1971	05	01	02	11	20.4	36.601N	110.481W	005G		2.00MLNOS
NOS	1971	05	06	16	57	18.1*	36.419N	113.084W	005G		2.20MLNOS
ERL	1971	11	04	02	18	58.7	35.220N	112.168W	005G		3.70MLERL
ERL	1971	11	10	11	14	09.6	37.707N	113.058W	005G		3.00MLERL
ERL	1971	11	10	13	38	14.3	37.684N	113.099W	005G		2.60MLERL
ERL	1971	11	10	13	46	55.0*	37.689N	113.075W	005G		2.20MLERL
ERL	1971	11	10	14	43	58.0	37.824N	113.058W	005G		3.50MLERL
ERL	1971	11	10	16	08	36.9	37.693N	113.042W	005G		3.00MLERL
ERL	1971	11	10	19	07	33.6*	37.704N	113.089W	005G		2.30MLERL
ERL	1971	11	10	19	41	33.4	37.834N	113.031W	005G		3.50MLERL
ERL	1971	12	15	12	58	14.5*	36.791N	111.924W	005G		3.00MLERL
ERL	1972	04	20	13	28	16.3	35.311N	111.640W	005G	3.70MB	
ERL	1972	06	26	20	06	51.7*	38.034N	112.798W	005G		
ERL	1972	11	16	02	17	46.8	37.676N	112.913W	010G		
ERL	1972	11	23	20	53	24.2*	37.506N	113.038W	005G		2.30MLERL
ERL	1973	02	09	17	38	37.0*	36.430N	110.425W	005G		3.20MLERL
ERL	1973	04	19	16	59	42.7	34.300N	112.617W	000	4.50MB	
GS	1973	07	14	10	54	01.0*	37.001N	112.913W	018		
GS	1974	03	14	20	59	57.2*	34.245N	112.699W	000G	4.10MB	
GS	1974	04	29	05	44	35.7	37.705N	113.026W	005G	4.10MB	3.00MLGS
GS	1974	04	29	07	35	51.8	37.814N	112.983W	005G	4.40MB	3.20MLGS
GS	1974	09	29	13	13	49.1*	33.601N	108.608W	005G		
GS	1974	12	20	03	01	10.4	33.860N	111.880W	004A		2.50MLGS
GS	1974	12	24	05	47	20.7	33.864N	111.879W	004		

Depth Control:

A	Assigned
G	Restrained by Geophysicist
N	Restraint at normal depth (33 km) when data are not sensitive to depth for a shallow focus.

Magnitudes:

M	Hypocenter based on macroseismic information
B	Parameters of hypocenter supplied by University of California at Berkley.
L	Parameters of hypocenter supplied by Lamont-Doherty Geological Observatory

3.2.4 Discussion of Figure 3, Seismicity Map.

Figure 3 is a computer generated plot of the earthquake epicentral locations described in Table 3.1. The majority of earthquakes are observed to occur along the Sevier, Hurricane and Paunsagunt fault zones (nothwest corner of Figure 3). Additional earthquake epicenters parallel the trend of the Mogollon rim (southwest to south central portion of Figure 3) although there is no clear relationship with mapped surface faults.

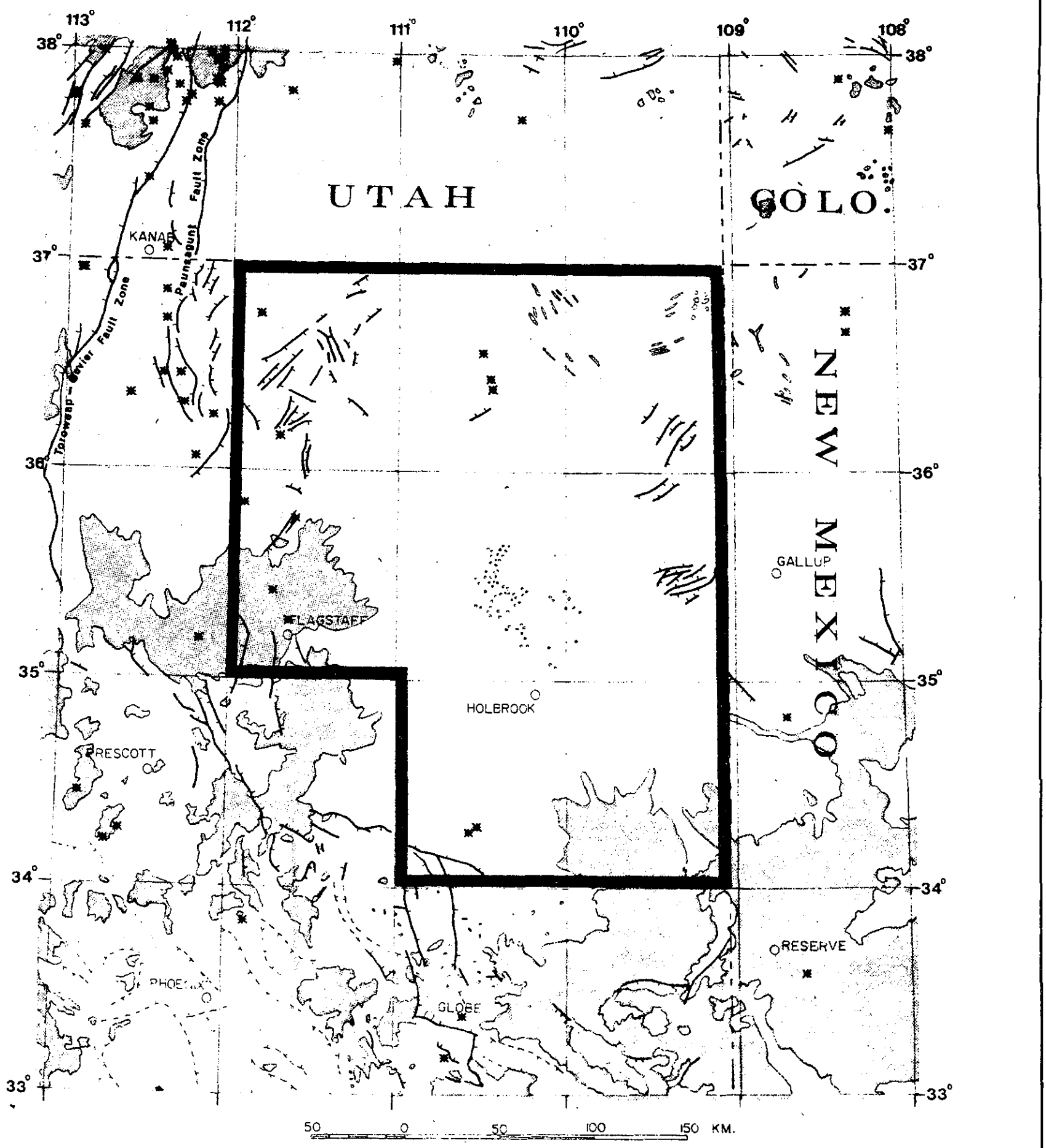

Fig. (3) Seismicity Map
Seismicity map showing epicentral locations for earthquakes, 1960–1974.

The association of some earthquake epicenters with the San Francisco volcanic field suggests an active tectonic environment.

The White Mountain volcanics of Arizona are apparently aseismic despite the youth (Pleistocene - Holocene) of the field. Macroseismic events are associated with the neighboring Datil Volcanic area of western New Mexico.

3.2.5 Interpretation of Seismicity Data.

As discussed by Smith and Sbar (1974), fault plane solutions for earthquakes occurring along the southern hurricane Fault Zone indicate primarily normal faulting with extentional or "T" axes oriented generally E-W or ENE-WSW. This suggests that the western boundary of the Colorado Plateau may currently exist in a state of net compression. This condition may arise as a consequence of intracontinental rifting (and attendent deformations such as ridge-ridge transform faulting in the Basin and Range Province) in response to the forces generated as a consequence of the interaction of the American and Pacific plates, the Jaun de Fuce subplate and the Yellowstone thermal Plume.

The reaction of the comparatively aseismic Colorado Plateau to these forces is uncertain. The association of two earthquake epicenters (36.430°N-110.425°W, 09 February 1973; 36.601°N-110.481°W, 01 May 1971) with the southern bifurcation of the Cow Spring monocline (Fig. 2 and 3) and the intersection of inferred north-south and northeast trending faults (Plate 7) suggests that stress is being actively released along zones of weakness in the Precambrian basement. The acquisition of earthquake fault plane solutions for the southern Colorado Plateau may reveal the stress environment of the Plateau and shed light upon the ability of the earth to laterally transmit stresses over appreciable distances.

3.3.1 Regional Bouguer Gravity Anomalies.

The regional Bouguer gravity anomalies associated with the U.S.G.S. study area are presented in Figure 4; the source of data is presented in Appendix 1, the method used to define them in Appendix 2. The Regional gravity field was used both to perform a regional - residual separation from the observed gravity anomaly data (Plates 2 and 3) and to ascertain if there are any

correlations of anomalous gravity with tectonic setting or volcanism as suggested by Drake (1969), Kaula (1969) and others.

3.3.2 Discussion of Figure 4, Regional Bouguer Anomaly Map.

The most prominent features of Figure 4 are the northwest trending isogal contours which reflect an increase in regional gravity to the southwest. Approximately 90 km northeast of Globe, Arizona, they achieve a maximum gradient of approximately 1 milligal per mile (.6 milligals/ kilometer).

The -190 milligal contour level separates the map into the "steep" slopes to the southwest and the broad gentle lows to the east and northeast.

A gravity minima of less than -220 milligals is found at the extreme eastern edge of the map, approximately 120 km northeast of Reserve, New Mexico.

A gentle east-trending positive anomaly is observed in the northwest corner of the area; it is flanked on the east by a broad, nearly circular gravity "low" with a value of

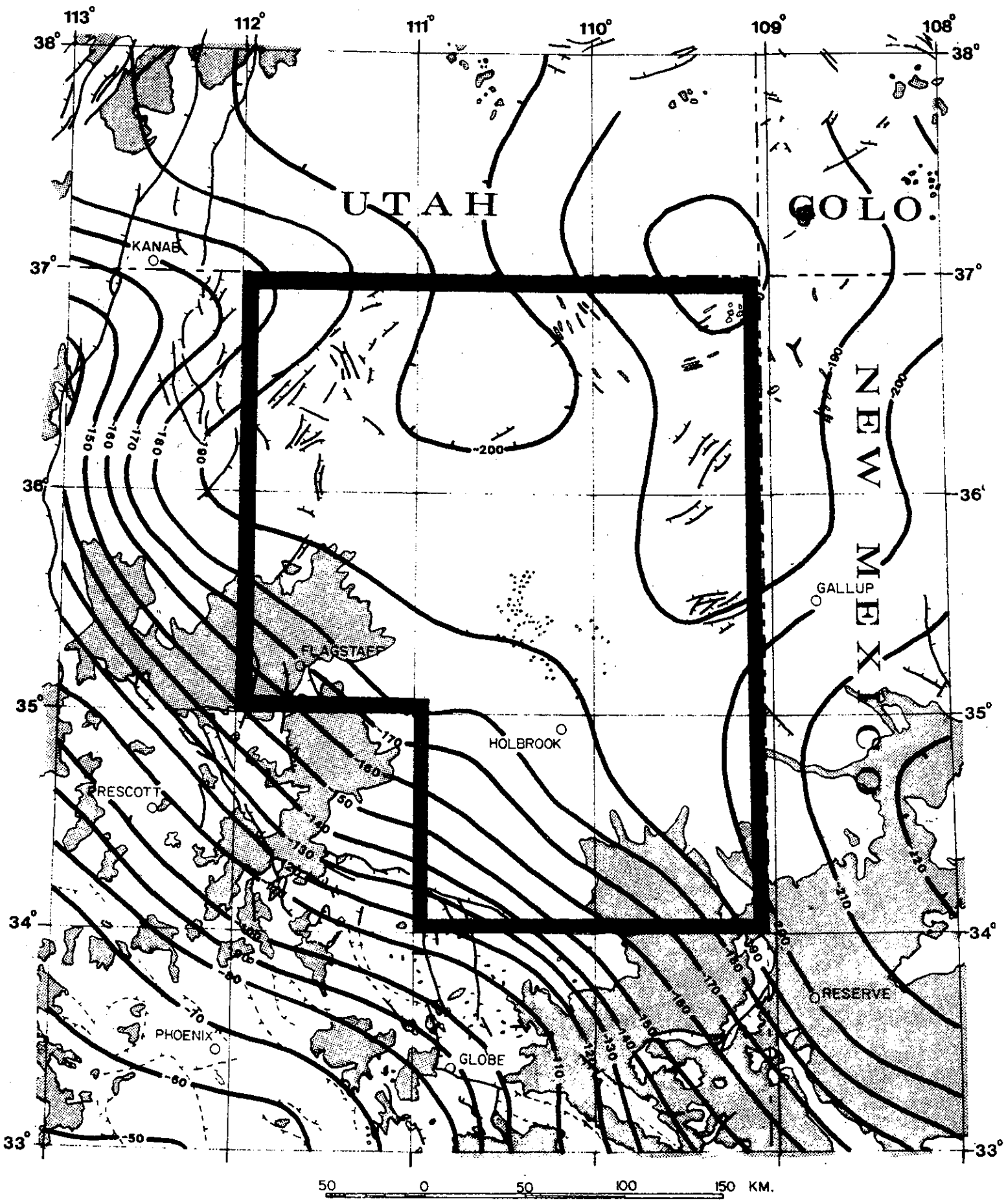

Fig. (4) Regional Bouguer Anamoly Map

-200 milligals. A circular, loacal "high" of approximately -180 milligals is associated with the northeastern edge of the study area.

3.3.3 Interpretation of Regional Bouguer Anomalies.

The regional Bouguer anomalies (Fig. 4) are interpreted as reflecting an increase in the thickness of the crust as one progresses to the north and east. The consequences of this increase are discussed in Section 8.2.2 and a model based upon this hypothesis is presented in Figure 16. This condition is thought to change in the southeast, however, where an anomalous crustal condition is thought to exist which may be related to an abundance of near surface, low density volcanic rocks coupled with an increase in incipient heat flow and a decrease in the depth of the Curie point isotherm causing the low Bouguer anomalies in the area and the observed departure of the field from the trends developed over the rest of the map.

The "high" closure associated with the northeast corner of the study area may be associated with the Defiance Uplift and the tectonic expressions of the Four Corners Platform and the Paradox Fold and Fault Belt.

In similar manner, the low closure at the northeastern (?) edge of the study area may be a reflection of the tectonic expressions the Kaiparowitz, Black Mesa and Henry Basin downwarps.

It is suggested that the departure of the field from its clearly defined trend is related to increasing crustal complexity near the northern edge of the study area and that this increasing complexity may be associated with increasing P_n velocities and decreasing crustal thickness (as described by Wollard, 1969) and provide an important input into the historical development of the Colorado Plateau.

3.4.1 Geothermal Gradient Data.

Regional geothermal gradient data, compiled from different sources, were reduced (as necessary) and contoured to create Figure 5. See Appendix 1 for data sources.

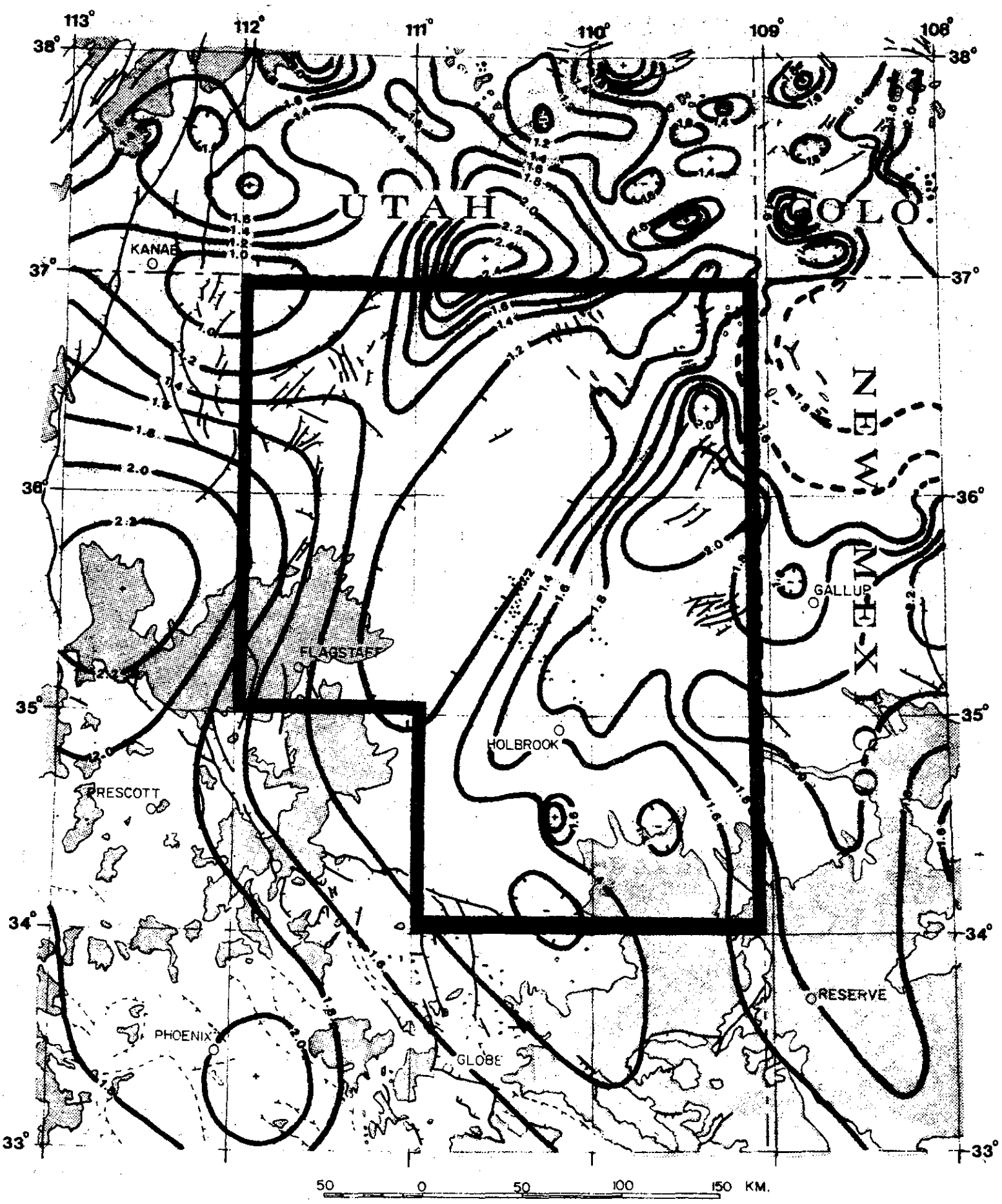

Fig. (5) Regional Geothermal Gradient Map

3.4.2 Discussion of Figure 5, Regional Geothermal Gradient Map.

The central portion of Figure 5 is dominated by a northeast-southwest trending geothermal gradient "low" which, east of Prescott, Arizona, abruptly swings to the southeast. The low is flanked on either side by gradient "highs." The eastern geothermal gradient "high" changes orientation from north-northeast above N35°, to south-southeast below. The western geothermal gradient "high", centered on N35°30', is quite circular. Its character changes to the south, however, where it swings to the southeast, parallelling the central low.

There is a large geothermal gradient "high", trending northwest, which is centered on the northern boundary of the study area.

A broad geothermal gradient "low", located to the southeast of Kanab, Utah, is elongated in an east-west sense.

Near the boundary between Utah and Colorado, there are numerous contour closures. This detail reflects the abundance of data available (in contrast to the relatively sparse data in northeast Arizona and northwest New Mexico).

This area, however, may be generalized as a broad gradient platform with an average geothermal gradient between 1.4 and 1.6°F/100 feet.

3.4.3 Interpretation of Regional Geothermal Gradients.

There is an apparently excellent correspondence between the regional geothermal gradients (Fig. 5) and the configuration of the Precambrian basement (Plate 7). For example, the southwest trending geothermal gradient "low" appears to be reflecting an increase in thickness of the sedimentary section associated with the large southwest trending basement trough interpreted from the geophysical data. Similarly, the geothermal gradient "highs" associated with the Defiance Uplift and Monument Valley are observed to relate spatially to interpreted basement "highs."

It is also suggested that the eastern boundary of the prominent southwesterly trending geothermal gradient "low" may reflect a change in regional lithologic properties relating to the boundary of the "old" Defiance Positive area (discussed in Section 8.1.2).

The validity of these observations is strongly tied to the uniformity of the thermal conductive properties of the rocks in the area. Empirically this assumption appears valid at least in the study area. It must be noted, however, that these observations are based upon a very limited number of datum points and an increased data sample is necessary to corroborate these preliminary conclusions.

4.0 LANDSAT MULTISPECTRAL IMAGERY

4.1 Introduction.

Standard LANDSAT multispectral imagery was acquired from the EROS Data Center. The imagery was selected on the basis of low sun angle, partial light snow cover and the absence of cloud cover; the following scenes were chosen:

Image I.D.	Date	Figure #
2370-17233	27 January 1976	7
5667-16315	14 February 1977	8
2369-17174	26 January 1976	9
2369-17181	26 January 1976	10
2369-17183	26 January 1976	11
1210-17264	18 February 1973	12
5272-16152	16 January 1976	13
2350-17130	07 January 1976	14

Low sun angle tends to accentuate features with subtle physiographic expression. Light snow cover also tends to enhance subtle features which may be of structural significance.

4.2 Data Processing.

Standard LANDSAT imagery was acquired as 7.3 inch positive transparencies (processed and corrected to a P-5 product) from the EROS Data Center. Black and white prints of bands 5 and 7 at scales of 1:1,000,000 and 1:500,000 and

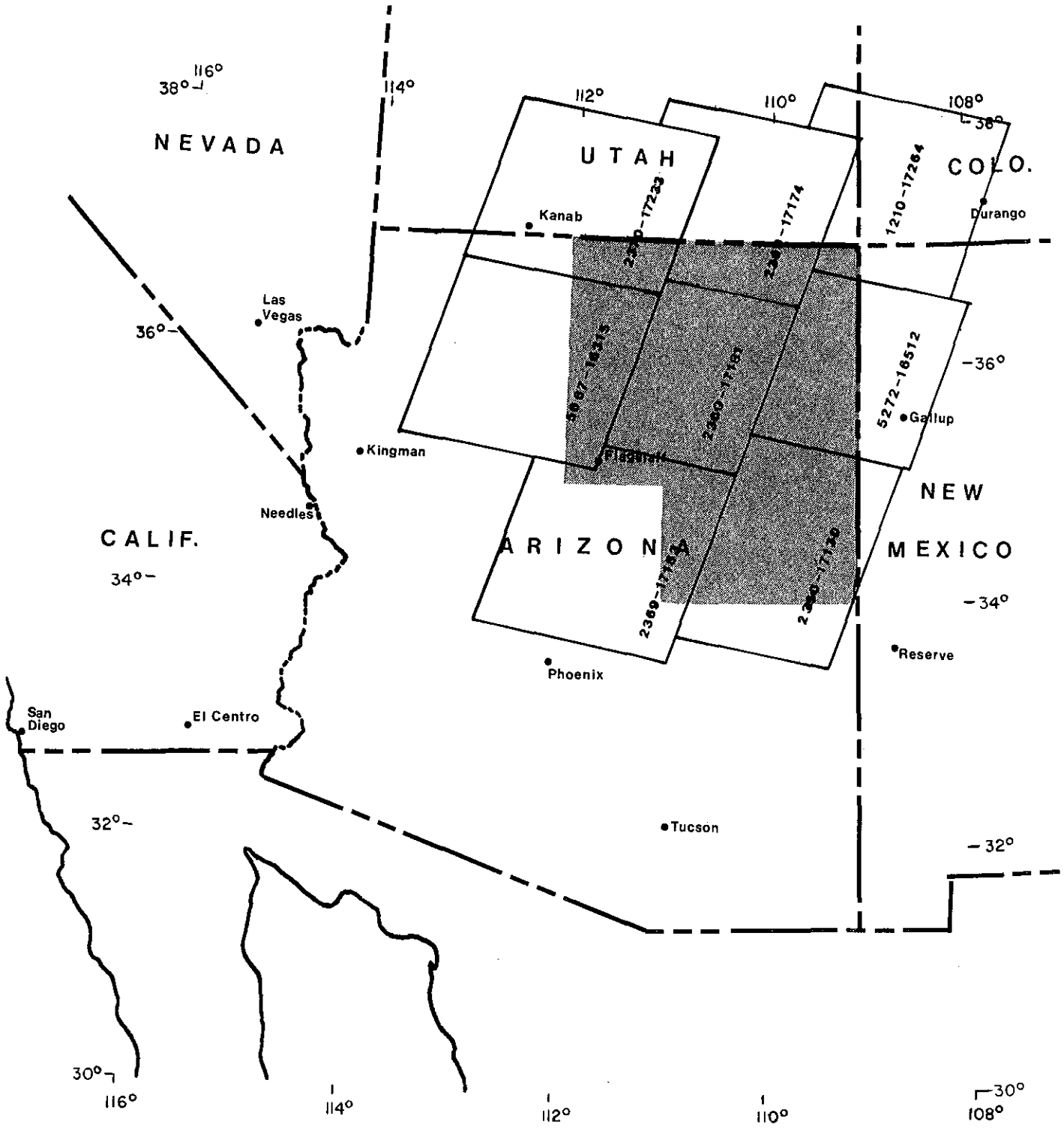

Location of LANDSAT Imagery

Fig. (6)
Index map showing locations of LANDSAT Imagery used in the study.

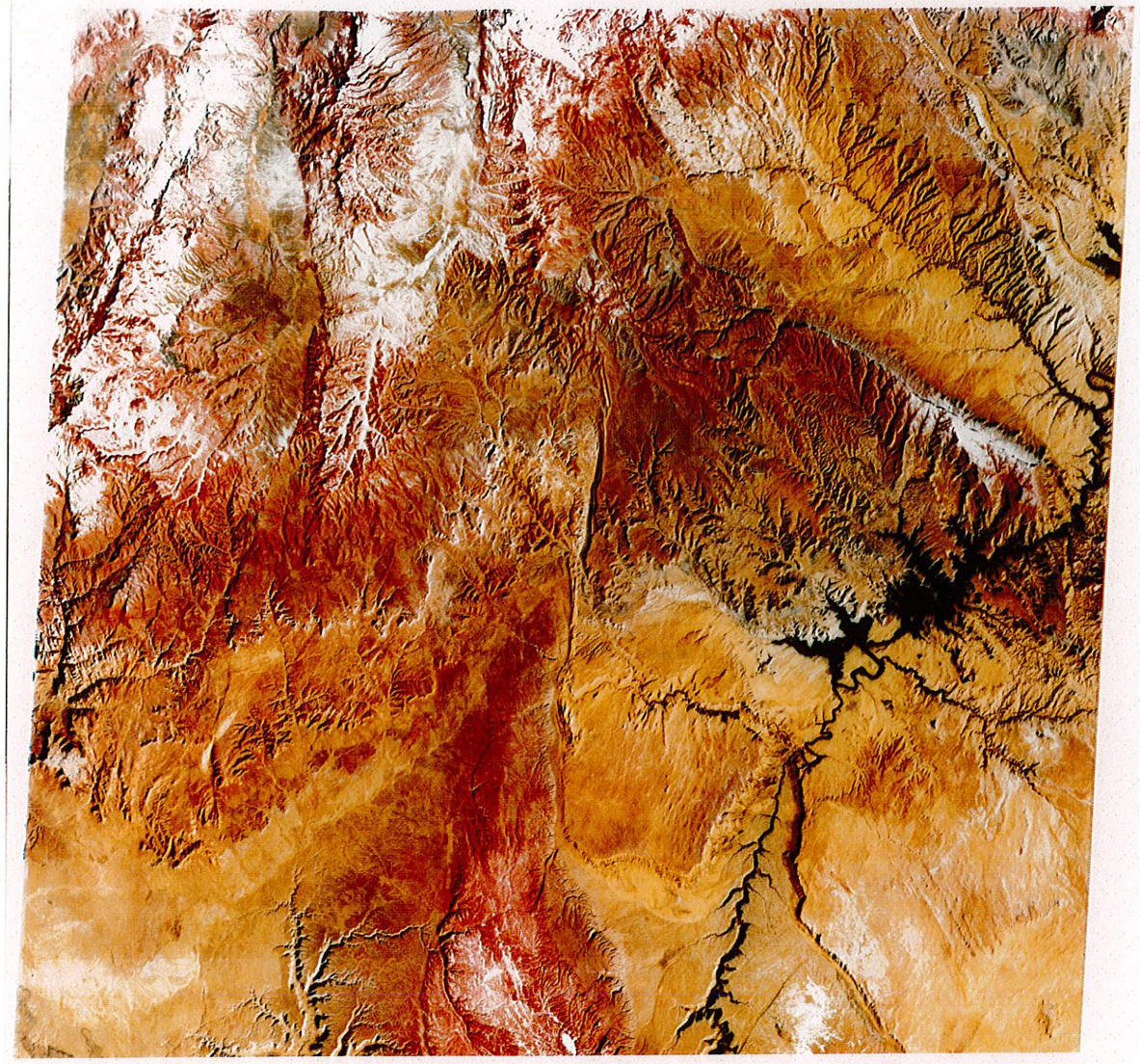

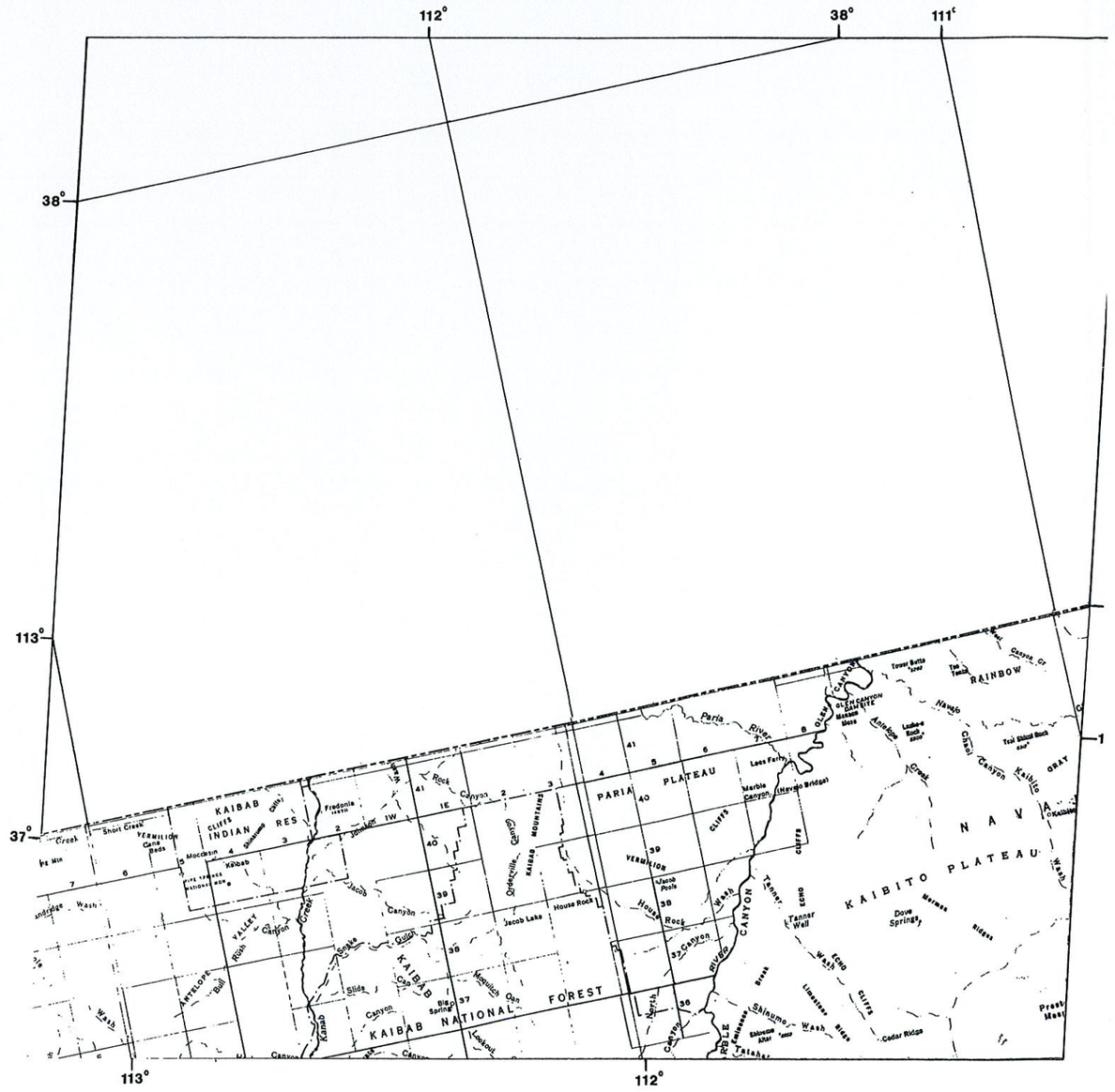

Scale 1:1000000

10 0 10 20 30 40 miles

10 0 10 20 30 40 50 km

Fig.(7) Landsat Image 2370-17233

W113-001 W112-301 W112-001
14FEB77 C N36-01/W112-25 D040-035 N N35-55/W112-11 M 45 ? D SUN EL23 AI27 SIS- P-N L2 NASA LANDSAT E-5 667-16315-5

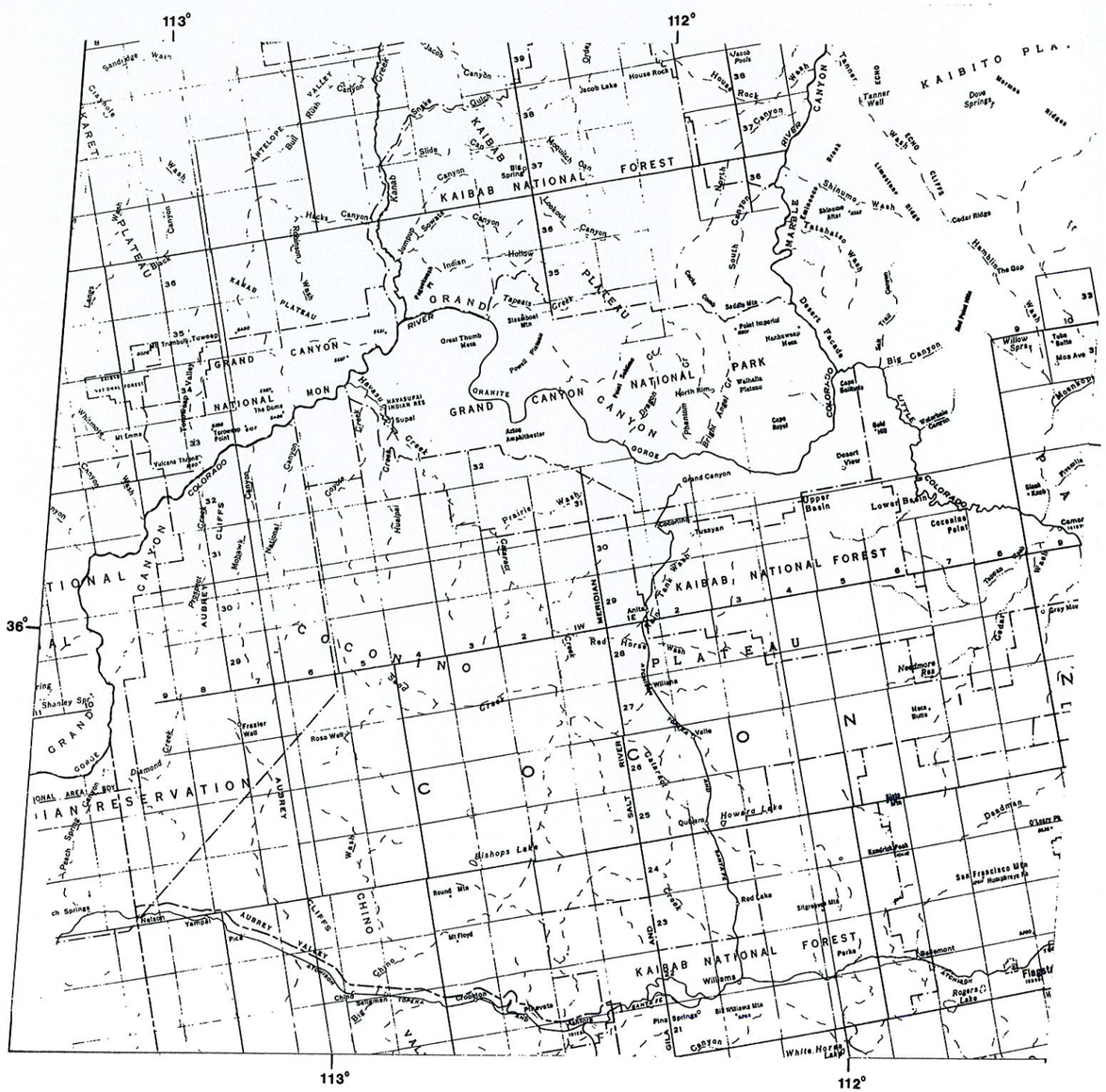

Fig.(8) Landsat Image 5667-16315

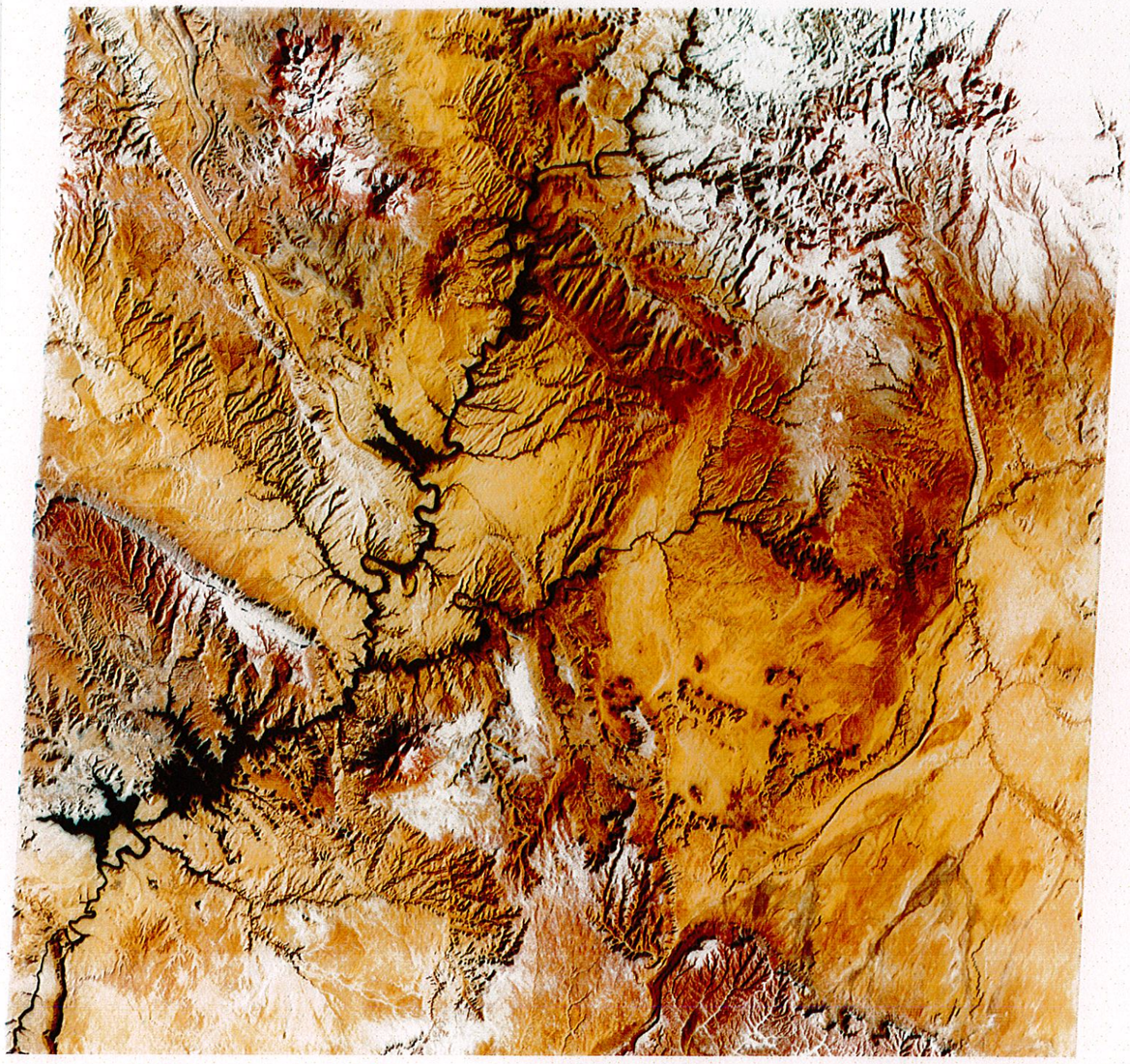

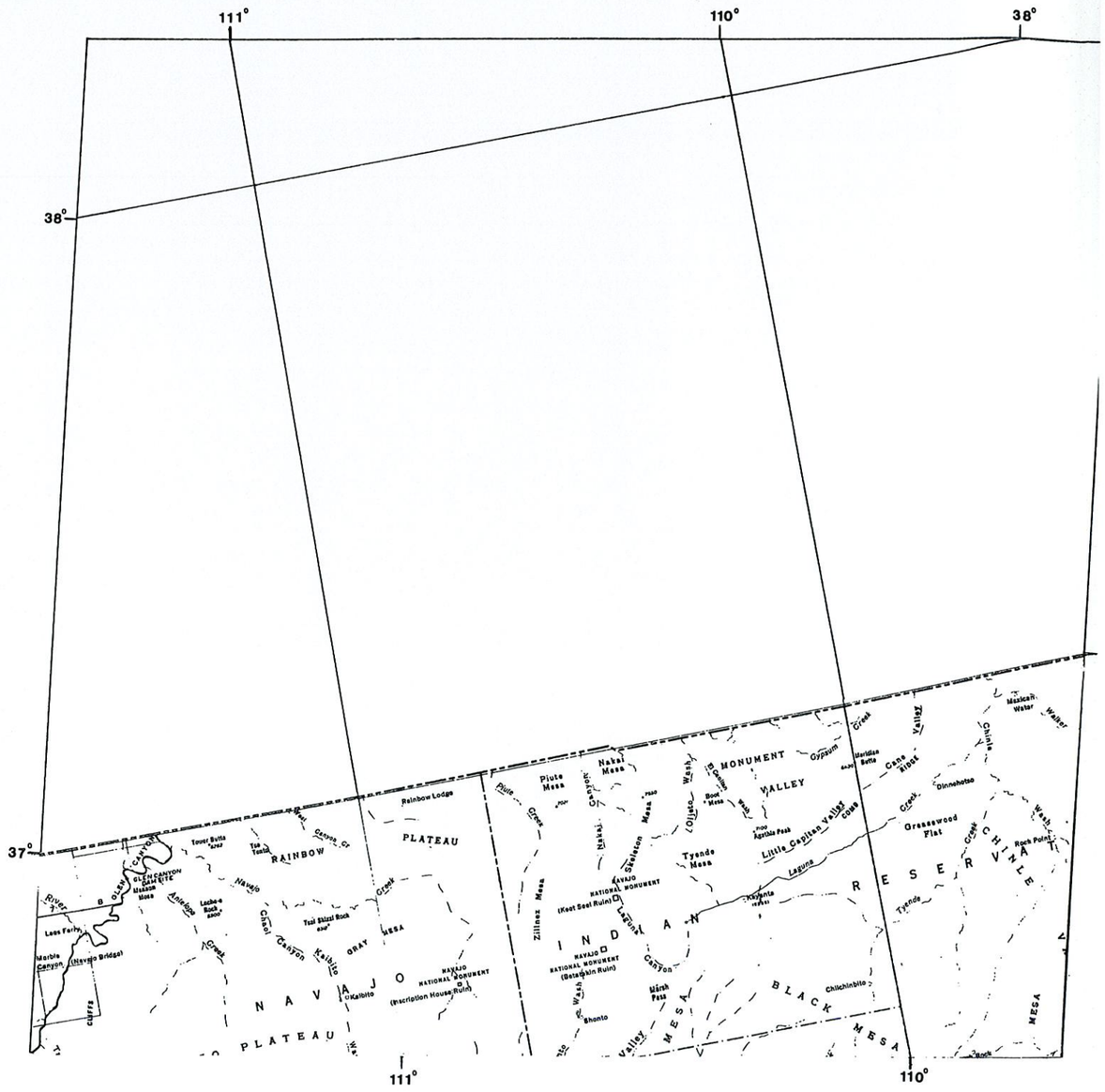

Fig.(9) Landsat Image 2369-17174

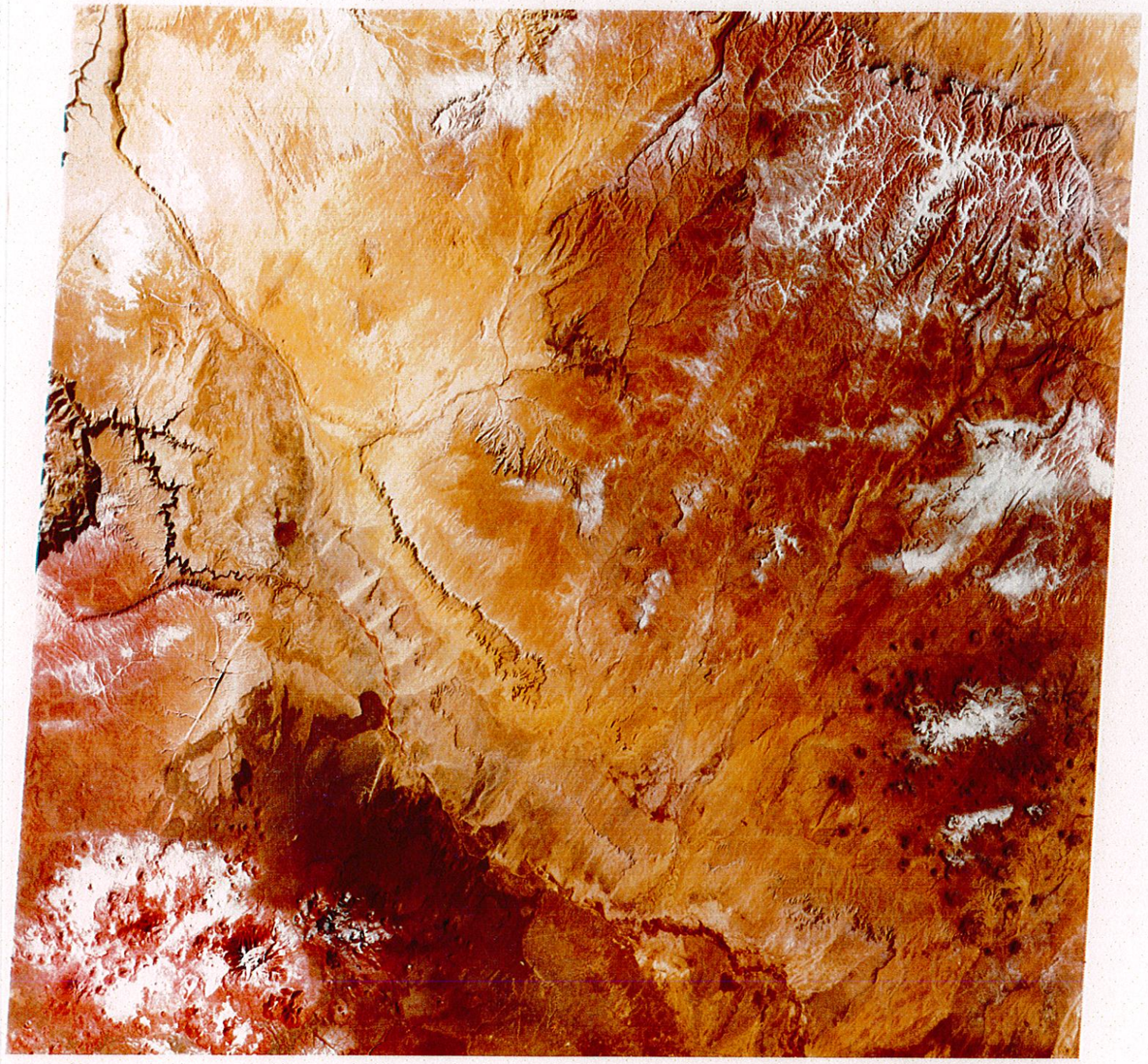

WIII-30| WIII-00| N035-00| IWI10-30
26JAN76 C N35-54/WI10-54 N N35-54/WI10-51 MSS 4 5 7 D SUN EL26 AZ143 191-5145-G-1-N-D-2L NASA ERTS E-2369-17181-5 01

Fig.(10) Landsat Image 2369-17181

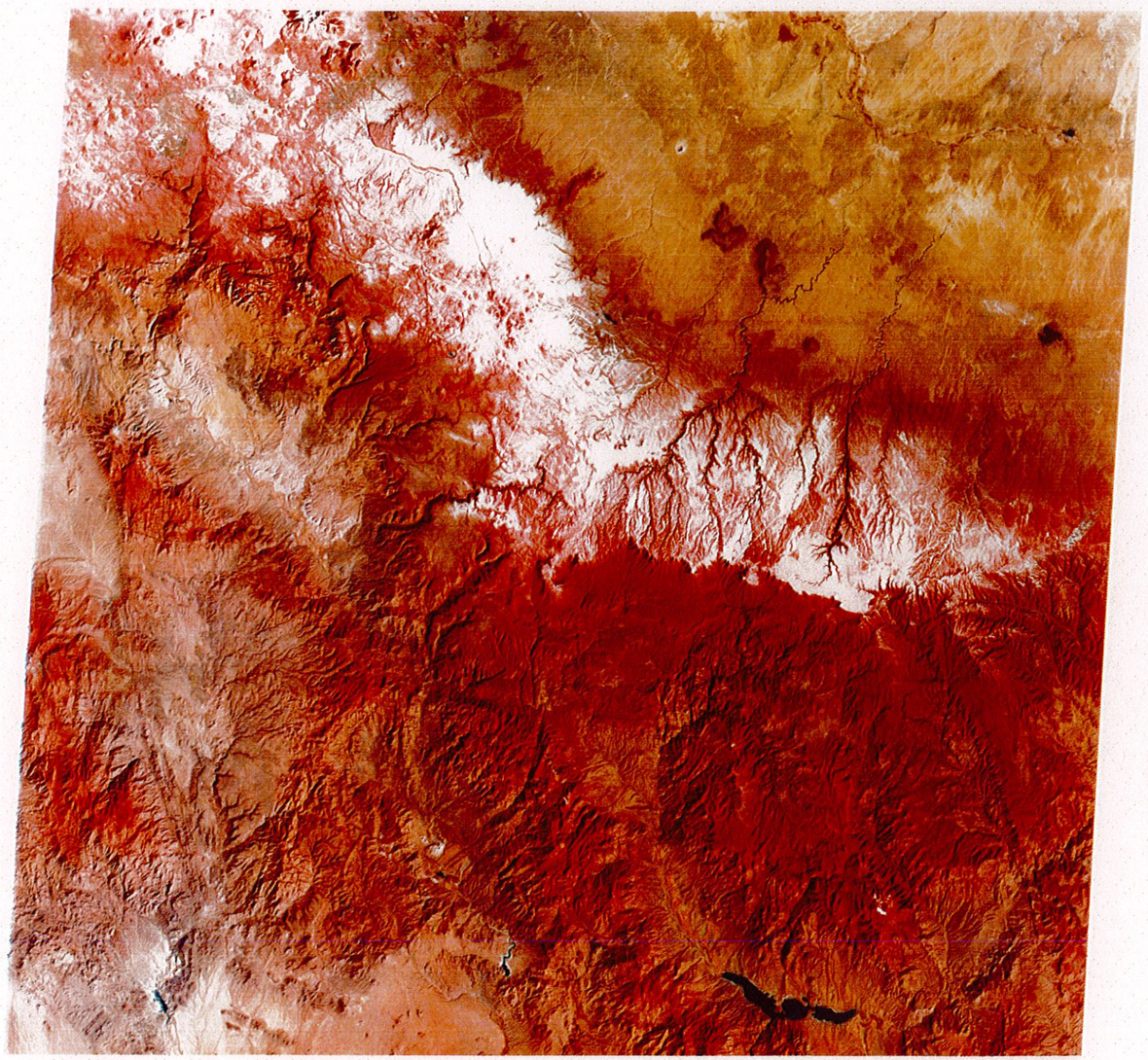

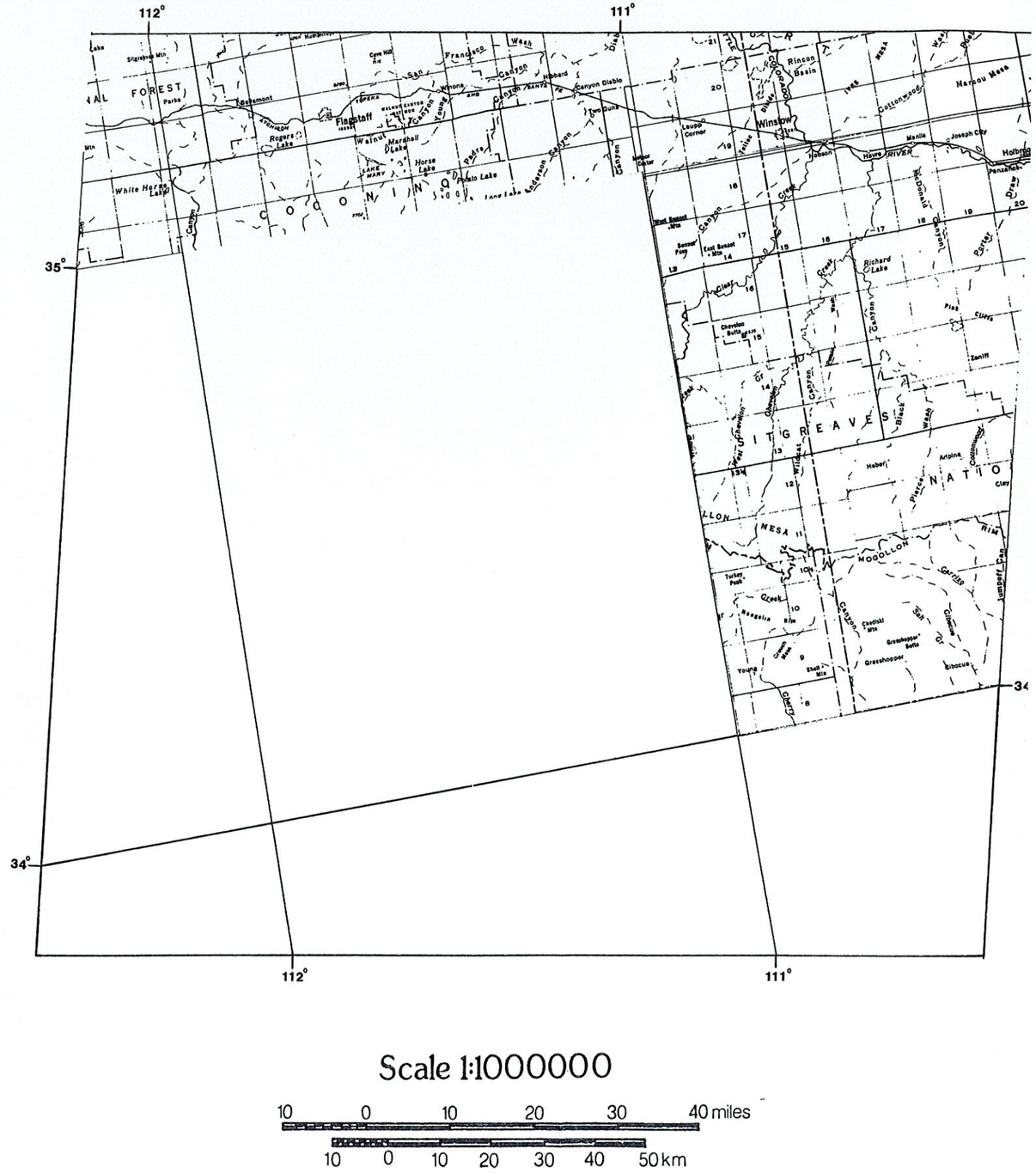

Fig.(11) Landsat Image 2369-17183

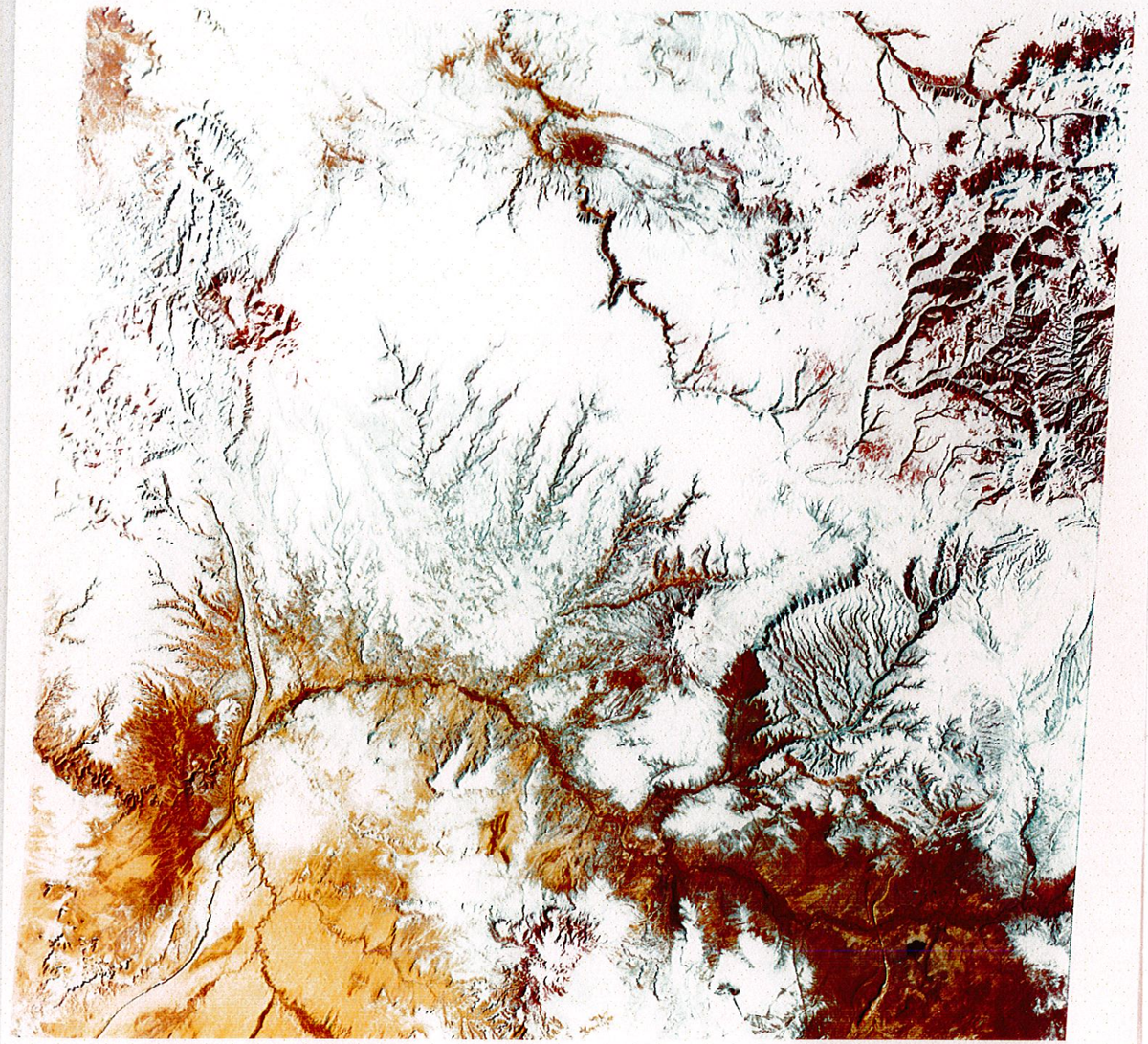

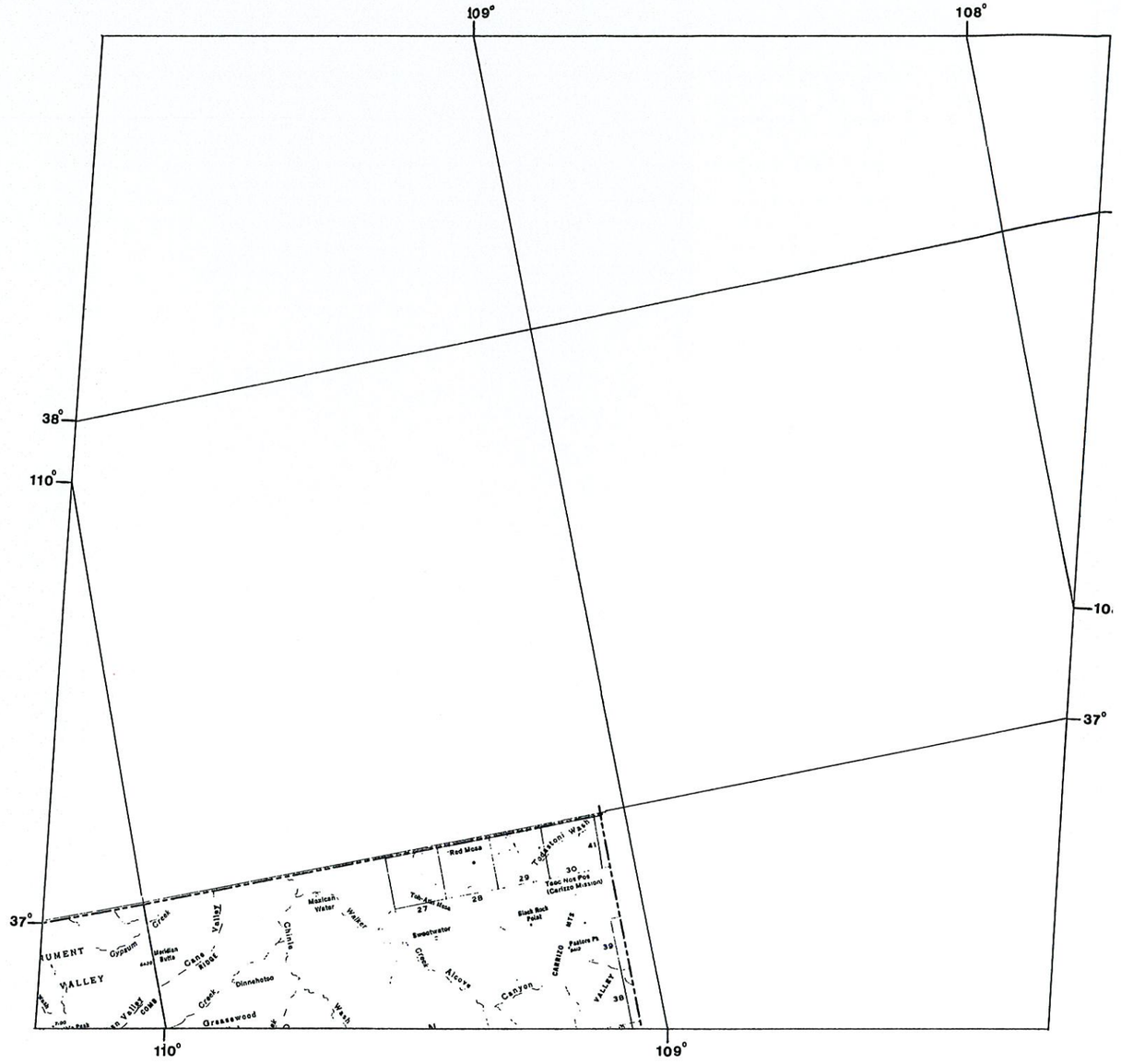

Fig.(12) Landsat Image 1210-17264

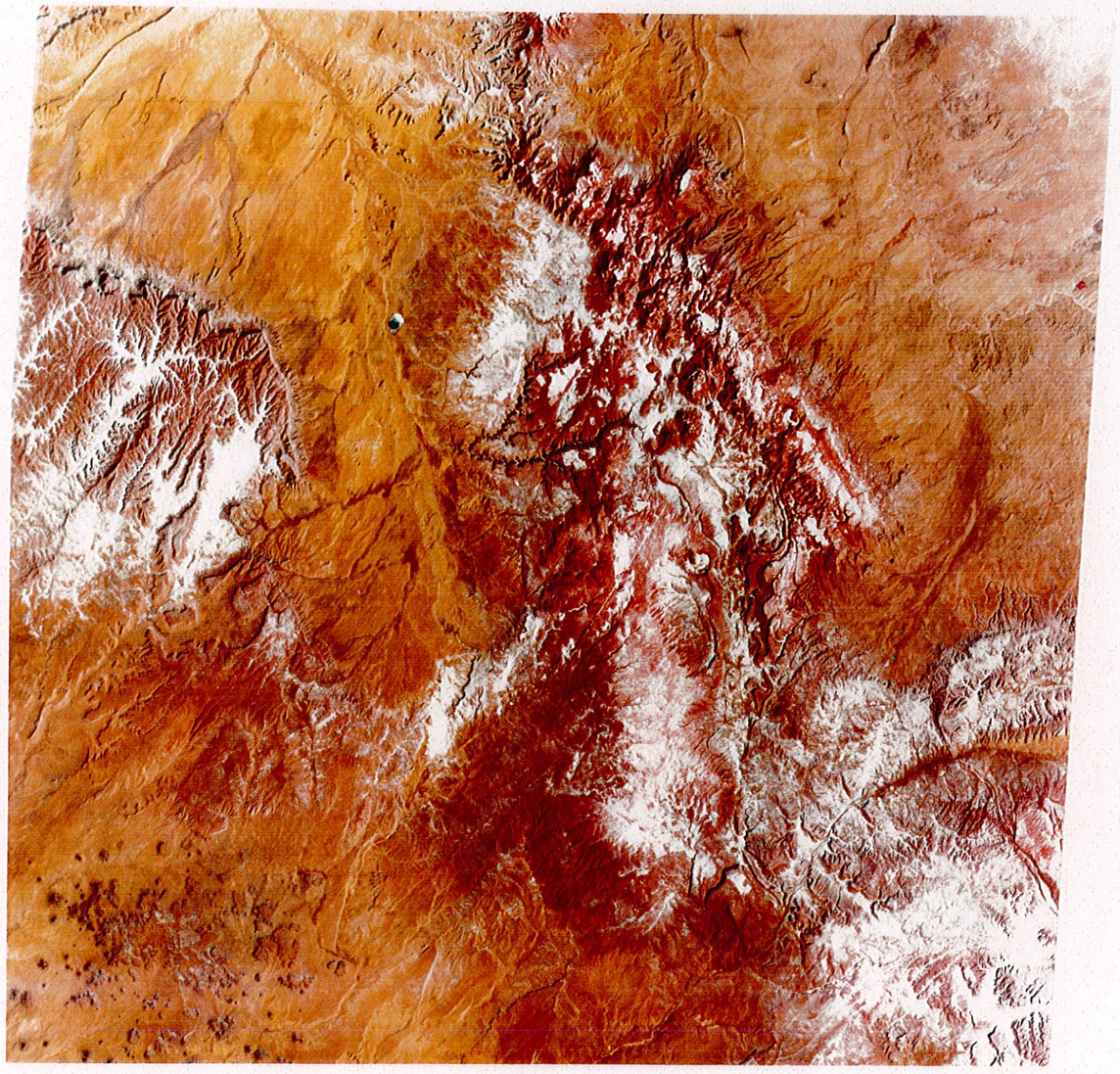

W110-001 W109-301 W109-001
16JAN76 C N36-00/W109-23 N N35-59/W109-22 MSS 45 7 D SUN EL22 AZ140 190-7737-G-1-N-D-2L NASA ERTS E-5272-16512-5 01

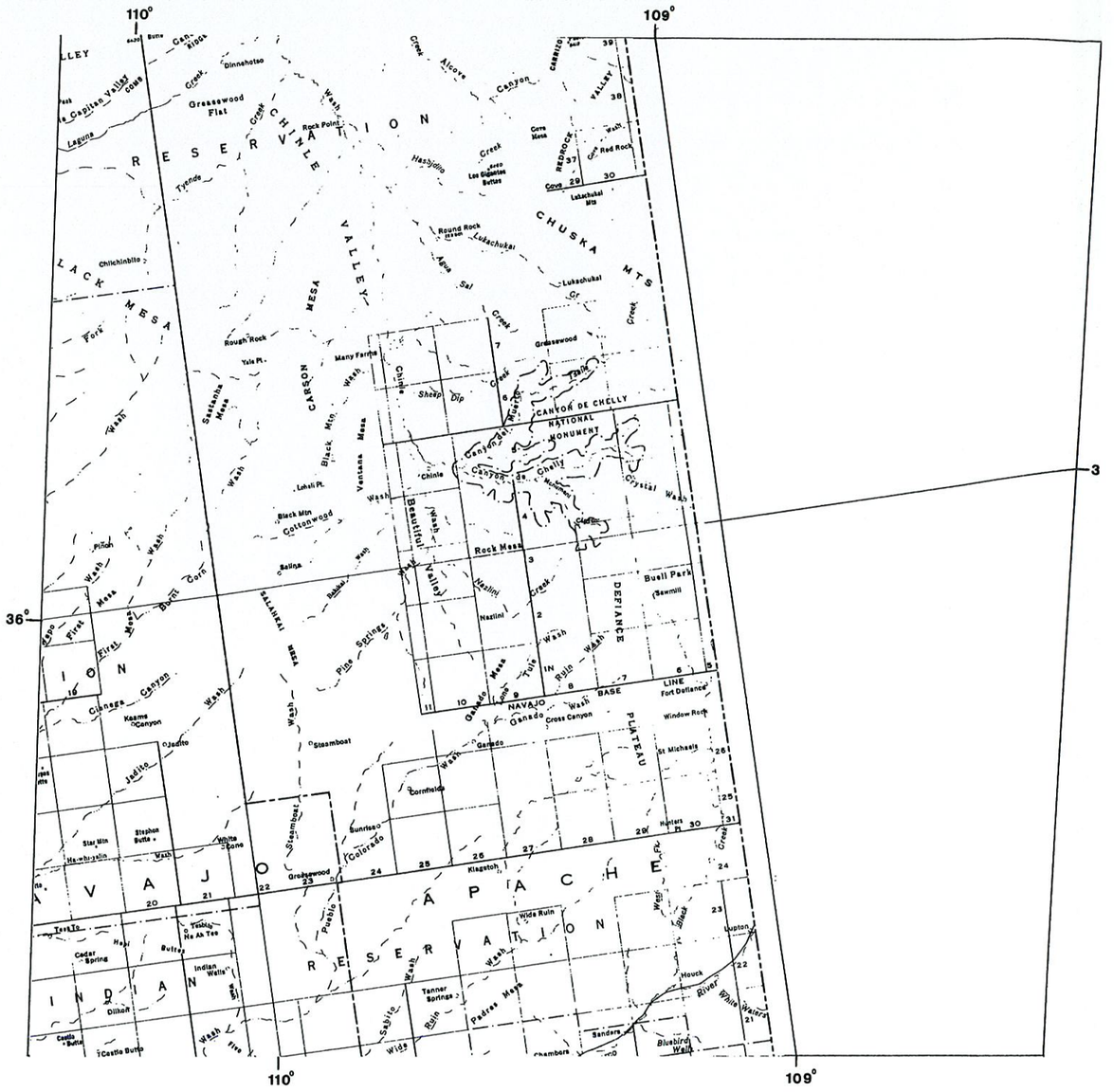

Fig.(13) Landsat Image 5272-16512

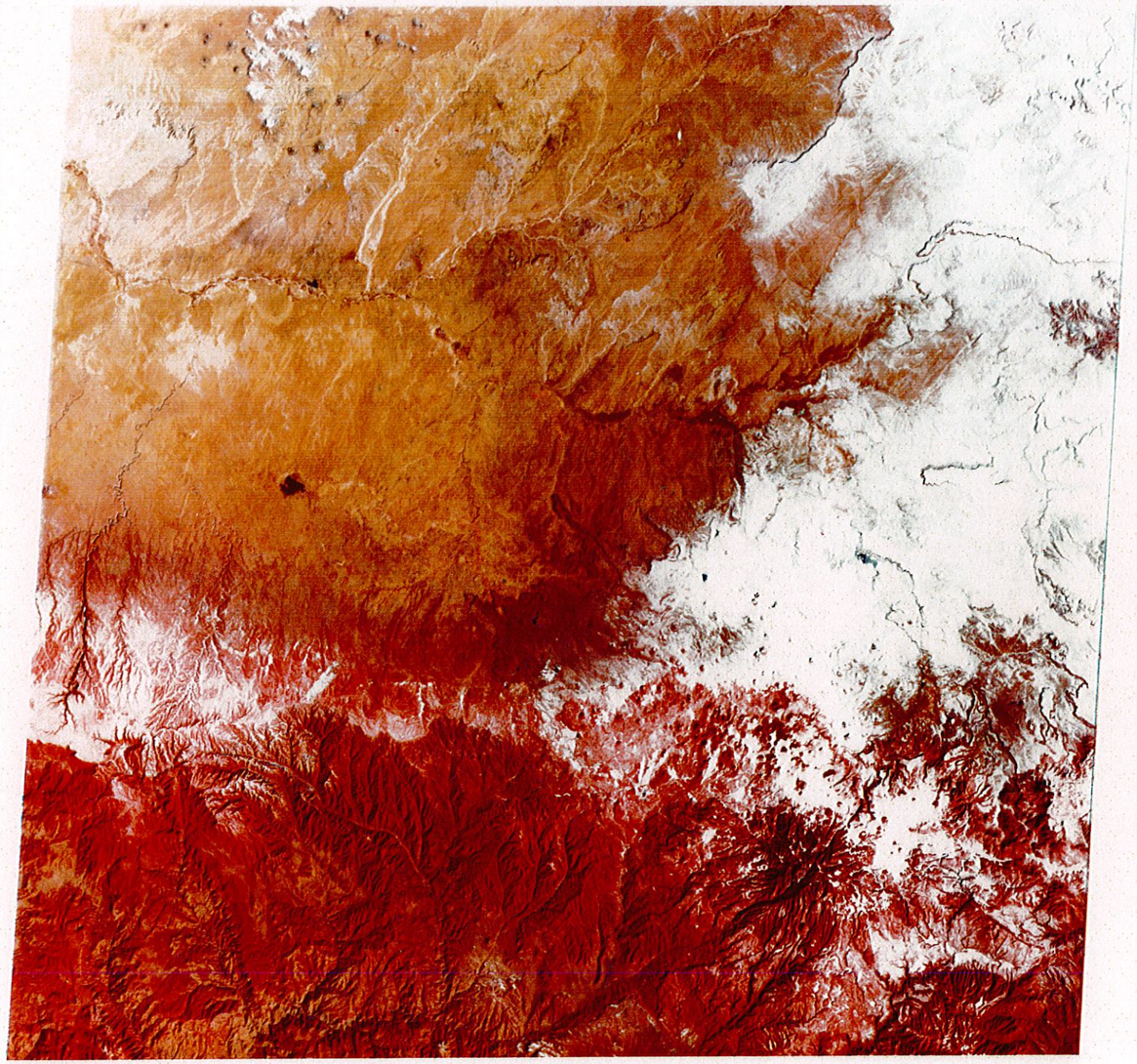

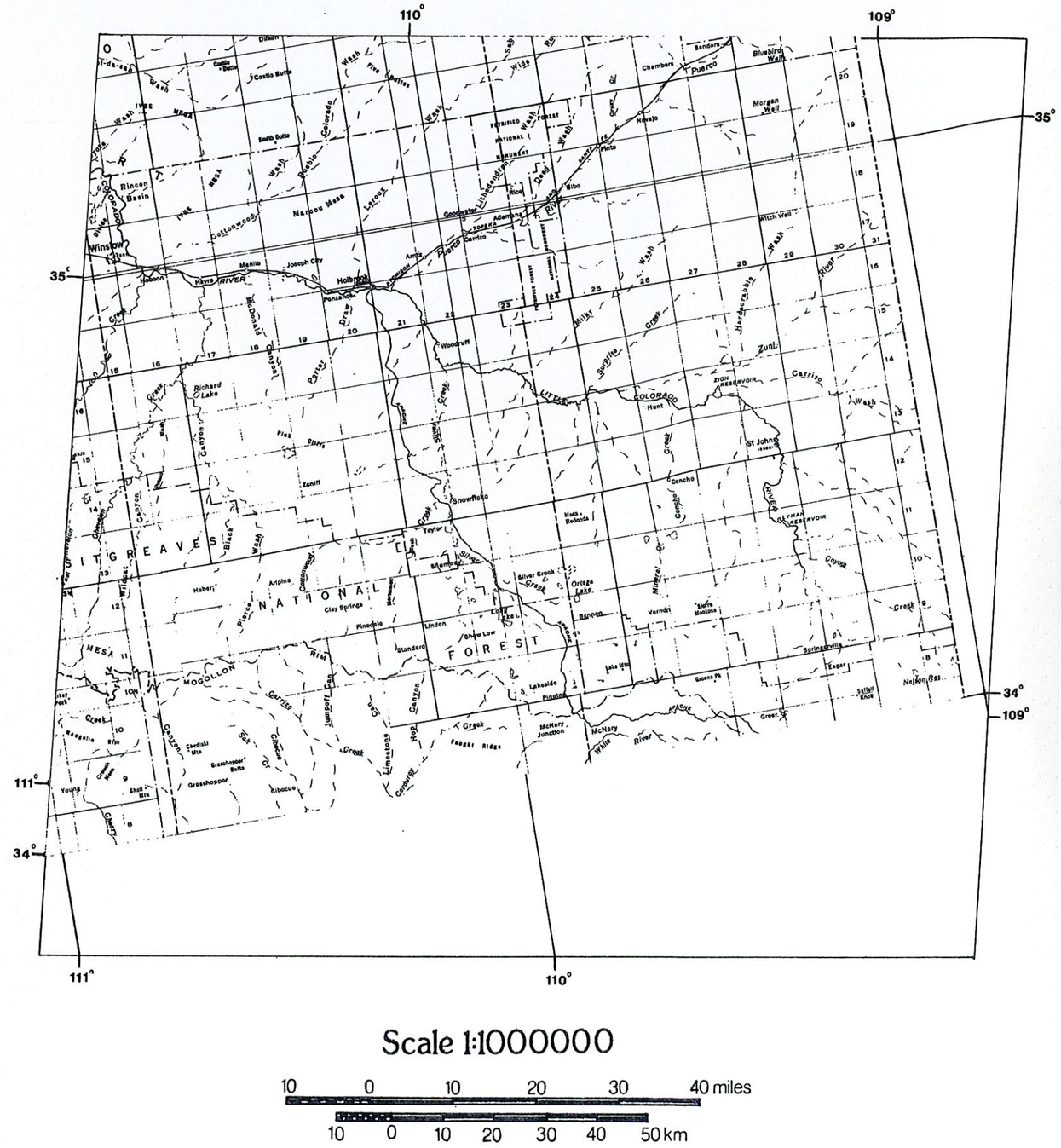

Fig.(14) Landsat Image 2350-17130

False Color composites, using bands 4, 5 and 7 (coded blue, green and red, respectively) at scales of 1:1,000,000 and 1:500,000 were prepared.

No attempt was made to "neutralize" the gray scale. A color balance was chosen which gave superior tonal discrimination. Film densities were controlled by exposure to bring out subtle tonal variations in bright areas while retaining detail in the shadows.

4.3 Data Interpretation.

A primarily structural interpretation of the LANDSAT imagery was performed through a process of repetitive mapping. Evaluation of the data was both monoscopic and steroscopic; the results of which are presented in Plate 2.

Three classes of structural elements have been derived based upon the process of repetitive mapping:

1. Probable faults which are clearly discernable - indicated by a solid line separated by a single dash.

2. Possible faults which are identified with "reasonable" certainty - indicated by a solid line separated by a double dash.

3. Indistinct or ambiguous structural elements associated with physiographic, geomorphic or color/tonal anomalies - indicated by a series of short dashes.

Repetitive mapping is a process of identifying significant structural trends by successive mapping of the imagery at different scales and product types. The results of this operation reduces, it is felt, the subjectivity in defining the more ambiguous structural elements.

Errors in locating the interpreted features on the map result from scaling errors in photo enlargement and transferring the data from image overlays and are considered to be relatively minor.

4.4 Discussion of Plate 2, "Structural Interpretation of LANDSAT Multispectral Imagery".

To the south of 35^{o} north latitude, structural lineaments predominantly trend northwest-southeast and tend to be expressed as color/tonal geomorphic anomalies. A prominent north-south striking (probable) fault, feature L36, is an important exception.

The dominant trend of structural lineaments associated with the San Francisco Volcanics is northeast to east-northeast. Here they appear to systematically cut volcanic centers such as Humphreys Peak (feature L32) or be associated with structural features and alignments of volcanic centers, craters and plugs (feature L29).

With the exception of the northwest quarter of the study area, the dominant structural grain is northeast. This trend is illustrated by features L15 and L16 which are the expressions of the axial traces of the steep limbs of the Comb and Cow Springs monoclines.

The northwest portion of the area is dominated by north-northwesterly trending structural lineaments which parallel the Echo Cliffs monoclines (feature L20). This trend is observed to continue to the south where it is expressed as a structural lineament associated with Ward Terrace.

The prominant southwest trending drainage patterns visible on the LANDSAT imagery are not directly represented on Plate 2. These remarkably linear washes are thought to primarily reflect the regional dip to the southwest.

5.0 INTERPRETATION OF BOUGUER GRAVITY ANOMALY DATA

5.1 Introduction.

Bouguer gravity anomaly data was evaluated as part of this study in order to gain insights into the density distribution and structural configuration of the subsurface. This data, acquired from several sources (see Appendix 1) were used to develop a data base from which plates 3, 4 and 6 were produced. The methods of treating the data as well as description of individual anomalies are discussed.

5.2 Treatment of the Data.

The pertinent gravity data selected for use in this study were reduced with a common density of 2.67 $gm\text{-}cm^{-3}$. This data were manually digitized by entering sufficient points to accurately describe the original contour maps. In this way, a data base was created which adequately described the observed Bouguer anomalies in the study area and permitted the placement of the data file onto a rectangular grid for surface to surface operations and contouring.

5.3 Observed Bouguer Gravity Anomalies.

Plate 3 is a map of the observed Bouguer anomalies in the study area. The anomalies range from a minimum of -250

milligals in the southeast corner to a maximum of -150 milligals in the northcentral portion of the map.

The map is cut by a northeast trending gradient in the field (OG1) which extends from the northeast to the southwest corner of the study area. It reaches a maximum gradient of approximately 5 milligals/mile east of Beautiful Valley. Anomalies to the south of the gradient generally trend east-west with occasional departures to the northwest (OG2).

A prominent, circular, -210 milligal "low" is centered southwest of Chevelon Butte (OG3). In the southwest (SE) portion of the area, a broad, -200 milligal "low" coincides with the White Mountain Volcanics (OG4).

To the north of the gradient, anomalies generally trend northeast and northwest. A -160 milligal north-northeast trending gravity high is centered on Beatutiful Valley (OG5). Hopi Buttes, in the center of the area, is associated with a large, northwest trending gravity low (OG6) which is flanked on the northeast by a northeast trending gravity "low" (OG7) and to the southwest, by a northeast trending gravity "high" (OG8).

In the northern part of the area, Monument Valley and Tyende Mesa are associated with circular and southwest trending "high" anomalies (OG9). The northern Kaibito Plateau, where data is very sparse, appears to be related to a broad, gentle "low" (OG10). At the southern end of the Kaibito Plateau, anomalies bifurcate, trending to the northwest and northeast.

The northwest edge of the Moenkopi Plateau is associated with a northeast trending -205 milligal "low" (OG11). South of this anomaly, a trend of N40^{O}E coincides with the San Francisco volcanic area where "lows" are associated with the majority of the volcanic centers (OG12).

5.4 Regional - Residual Separation.

The purpose of defining the residual Bouguer anomalies is to remove the influence of the regional field (described in Section 3, and Appendix 2), thereby separating the effects of local bodies masked by the regional field.

The philosophical basis of the regional-residual separation is found in the concept that observed Bouguer anomalies are a composite of the effects of local anomalous masses and large scale crustal features. This leads naturally to a definition of the residual anomaly:

$$g_{residual} = g_{observed} - g_{regional}$$

The subtraction of the observed from the regional anomalies is operationally performed on the gridded data (Appendix 2); the result is a residual anomaly map.

5.5 Residual Gravity Anomalies.

Plate 4 is a map of the residual Bouguer anomalies in the study area; anomalies vary between (approximately) plus and minus 30 milligals.

As in the case of the observed anomaly map, this map is also cut by the northeast trending gradient described in Section 5.3 (RG1). It is, however, observed to broaden in the vicinity of Holbrook, Arizona, becoming less clear. The maximum gradient characteristics of this anomaly are, however, preserved.

A northeast trending, +20 milligal gravity "high", centered on St. Johns, Arizona, exhibits minor nosing to the northwest (RG2).

In the extreme southeast portion of the map, a northwest trending gravity "low" is associated with the White

Mountain volcanic area (RG3). To the north of Springerville, Arizona, the trends of anomalies reorient from northwest to northeast (RG4).

A reorientation of the field is observed to the west of Cibecue, Arizona, where east-west trending anomalies swing north-south (RG5). A circular -20 milligal anomaly, centered near Chevelon Butte, defines the western extremity of this reorientation (RG6).

Toward the center of the area, the Hopi Buttes are associated with northwest trending gravity minima (RG7); this trend shifts abruptly to the northeast in the vicinity of Antelope Mesa (RG8).

The San Franciso volcanics are related with -15 to -20 milligal anomaly "lows" which trend N40^{o}E (RG9).

To the north of Flagstaff, Arizona, anomalies trend northeast until, at the southern edge of the Mormon Ridge fault zone, they bifurcate, one set maintaining the northeast trend while the other assuming the northwest trend of the Echo Cliffs Monocline (RG10, RG11).

The +20 milligal anomaly associated with Monument Valley (RG12) is flanked on the west by a +30 milligal anomaly (RG13). Together they define the east and west edges of a southwest trending "high" anomaly platform associated with the Comb and Organ Rock monoclines.

Twenty miles east of the Four Corners region, an elongated east-west trending gravity high is observed (RG14).

The Carrizo Mountains relate to the northern edge of a northeast trending +20 milligal anomaly spatially associated with Redrock Valley (RG15).

Beautiful Valley is associated with a north-northwest trending +30 milligal gravity anomaly (RG16).

5.6 Interpretation of Gravity Data.

The northeast trending gradient (RG1) is interpreted as reflecting a pronounced fault or discontinuity in the rocks of the Precambrian basement. The similarity of anomaly wavelengths on either side of the fault suggests that throw on the fault (inferred as downthrown side to the northwest) is minimal and the anomaly arises primarily

from the density contrast between basement blocks separated by the fault.

The positive anomaly near St. Johns, RG2, is interpreted as reflecting arching in the basement which is bounded on the south by a northeast trending fault (or fault zone).

The pronounced -25 mgal "low" (RG3) in the White Mountain volcanic area is interpreted as a basement "high" composed of anomalously low density material, possibly a batholithic intrusion. The northwest and northeast trending anomalies immediately to the north suggest that faults control the orientation of basement blocks of varying density.

The reorientation of the field in the vicinity of Cibecue (as expressed by anomalies RG5 and RG6) is probably associated with the Chevelon Creek-Holbrook Buckle where a change in the mapped regional structural trend occurs. The LANDSAT data suggests that this is an area of great structural complexity.

The gravity minima (RG7) associated with the Hopi Buttes volcanic area probably reflects the presence of low density materials in the crust. The northern edge of this anomaly appears to be fault bounded and it is this fault which probably controls the trend of RG8.

The gravity lows associated with the San Francisco volcanic area (RG9) are interpreted as representing fault controlled, anomalously low density materials in the upper crust. It is conceivable that they may reflect the existence of batholithic intrusions.

The anomalies associated with the Monument Valley area are interpreted as reflecting a basement "high" (RG12) bounded to the south by a northeast trending fault (downthrown side to the southeast) which corresponds with the trace of the Comb and Organ Rock monoclines.

The elongated, east-west trending anomaly (RG14) may arise from the topography of the Precambrian basement, influenced by the presence of highly magnetic bodies (with little or no apparant density contrast) in the crust.

The Beautiful Valley anomaly (RG16) is interpreted as resulting from a complexly fault-bounded basement block with a strong positive density contrast.

6.0 INTERPRETATION OF AEROMAGNETIC DATA

6.1 Introduction.

Aeromagnetic anomaly data was evaluated as a part of this study primarily to define the structural configuration of the magnetic basement.

The data used for this task was derived from a digital tape of Sauck and Sumners' Aeromagnetic Survey of the State of Arizona, flown between June 1 and August 21, 1968 (Sauck and Sumner, 1970).

6.2 Treatment of the Data.

Prior to gridding and contouring the data (Appendix 4), the flight lines were sorted and spurious data points identified and deleted. Because the survey was flown at two different elevations, 9000 and 11000 feet, (Sauck and Sumner, 1970) and because it was desirable to view the data as a continuously contoured map, it was decided to downward continue the higher elevation data by 2000 feet. The location of the downward continued portion of the map is identified on Plate 5, the method used is discussed in Appendix 3). 400 gammas was then subtracted from the data to return the data to a 0 gamma datum (the U of A data is recorded as gamma plus 400).

6.3 Residual Magnetic Anomalies.

Plate 5 is a map of the residual magnetic anomalies in the Study Area. Residual magnetic intensity values range from more than +1500 gammas in the Canyon De Chelly area to less than -300 gammas north of Sunseta Buttes (approximately 10 miles southeast of Canyon De Chelly).

With the exceptions of the Canyon De Chelly, Red Mesa, White Mountain and the San Francisco Mountain areas, the residual anomalies are characteristically broad, low frequency events. The above areas are associated with high frequency and amplitude anomalies with varying trends.

The trends of anomalies in the rest of the area vary widely; northeast-southwest, northwest-southeast, north-south and east-west are represented. By far the east-west trend is the most abundant.

Magnetic anomalies define a northeast trending linear zone (M1) which corresponds spatially with the gradient in the Bouguer gravity data (RG1). This trend is locally disturbed or broken, usually by anomalies trending northwest (M2 and M3 for example). M2 corresponds (spatially) with Beautiful Valley.

A very prominent east-west trending "high" is observed at the extreme northeast corner of the study area (M4).

South of the northern slope of Black Mesa is a large, broad magnetic "low" with -200 gammas of relief (M5). Immediately to the northwest of this anomaly, the isogam contours define a northeast linear trend which corresponds with the Cow Springs Monocline (M6).

In the vicinity of the San Francisco Mountains, local magnetic highs appear to be associated with individual volcanic centers (M7 and M8 for example). The same phenomenon is observed in the White Mountain volcanic area. (M9). Despite the circular and east-west character of individual anomalies in the Flagstaff area, a gross northeast trend is observed as exemplified by anomaly (M10).

6.4 Interpretation of Magnetic Anomaly Data.

A linear anomaly pattern (M1) extends from the northeastern to the southwestern edges of the study area. This pattern is interpreted as reflecting an extensive fault zone in the Precambrian basement which separates rocks of dissimilar susceptibilities without significant vertical dis-

placement (as determined by the similarity of anomaly wave lengths on either side of the zone).

This pattern is locally distributed by anomalies trending (generally) northwest (M2, M3) which are in turn, interpreted as reflecting faults which generally offset M1. This offset is apparently left lateral and probably represents a dip-slip component of movement along normal faults.

High amplitude anomalies such as the one located to the west of M1 and M4 are probably associated with circular bodies with high susceptibilities which appear to have little or no gravity expression. Their association with basement structural "highs" (Plate 7) suggests that they may be related to intrabasement features such as laccolithic intrusions or domes.

7.0 CONFIGURATION OF THE PRECAMBRIAN BASEMENT

7.1 Configuration of the Precambrian Basement.

As interpreted from the aeromagnetic data, the topography of the Precambrian basement is quite irregular. It achieves its lowest elevation, 820 meters below mean sea level, in Cane Valley to the east of the Comb monocline and its highest elevation (1750 meters above mean sea level) to the north of Mt. Baldy in the White Mountains.

Each volcanic area, the San Francisco Mountains, Hopi Buttes, and the White Mountains, appears to be associated with arching in the Precambrian basement as well as positive (surface) topographic expression. This arching could be responsible for (or contemporaneous with) the faulting (or the rejuvenation of old faults) observed to be associated with each area.

The western and southern boundaries of the Defiance Plateau appear to be closely associated with faults interpreted from the geophysical data. In addition, the western edge of Lukachutai Mountains and the Carrizo Mountains block

seems to be closely associated with faults. This strongly suggests that faulting may have played an important part in the development of the broad asymmetrical anticlinorium of the Defiance Uplift.

The basement appears to be divided into regular, fault bounded blocks that trend (predominantly) northeast-southwest. The average width of these blocks is approximately 40 kilometers and they tend to be terminated by north-south and northwest-southeast trending faults. The edges of several blocks correspond with monoclinal segments and LANDSAT structural lineaments (or the terminations of same). It is conceivable that many of the interpreted basement faults may represent basement contact zones rather than zones of displacement. As such, their geophysical signatures arise from the susceptibility and density contracts between the blocks without the influence of vertical displacements between them.

8.0 SUMMARY AND CONCLUSIONS

8.1 Discussion of Implications to Structural Geology.

8.1.1 Monoclines of the Southern Colorado Plateau.

Baker (1935), Kelley (1960), Davis (1975) and others have speculated that the monoclines represent the draping of the sedimentary section over high angle reverse or normal faults in the Precambrian basement. Most workers assign an age of late Cretaceous early Tertiary (Laramide Age) to this episode of deformation.

As a result of this study and corroborated by the work of Case and Joesting (1972) it is concluded that many of the major monoclines (the Comb, Echo Cliffs and Cow Spring monoclines, for example) indeed appear to be associated with faulting in the Precambrian basement of the Colorado Plateau.

Kelley (1960) and Davis (1975), among others, have speculated that alignments and/or terminations of monoclinal segments define a regional basement fault pattern that divides the Plateau into a great number of regular blocks. The results of this study, as well as the findings of Case and Joesting, tend to substantiate this hypothesis (see Plate 7) and while there is not a direct correspondence between the hypothesized fault system and the interpreted

basement pattern, there does appear to be good correspondence in the represented trends.

8.1.2 Defiance Positive Area.

The Defiance Uplift of approximately Laramide age is superimposed upon the Defiance Positive Area of Paleozoic (or posibly older) age. This area remained essentially above sea level until the Permian period. The approximate location of the Defiance Positive Area during the Cambrian era is identified in Figure 15 (adapted from Wilson, 1962). Also shown on Fig. 15 is the location of interpreted faulting, the geophysical expressions of which are discussed in Section 4.5, 5.5, 5.6, 6.3 and 6.4. It is suggested that this fault or fault zone represents the ancestral boundary of the Defiance Positive Area and that the relative physiography of the area was controlled by movements along this and associated fault systems from Precambrian through Permian time. Evidence that portions of this fault have been rejuvenated since the end of the Paleozoic era is observed in the LANDSAT imagery where structural lineaments are observed to relate (spatially) to the trace of the basement feature and from geologic mapping where mapped

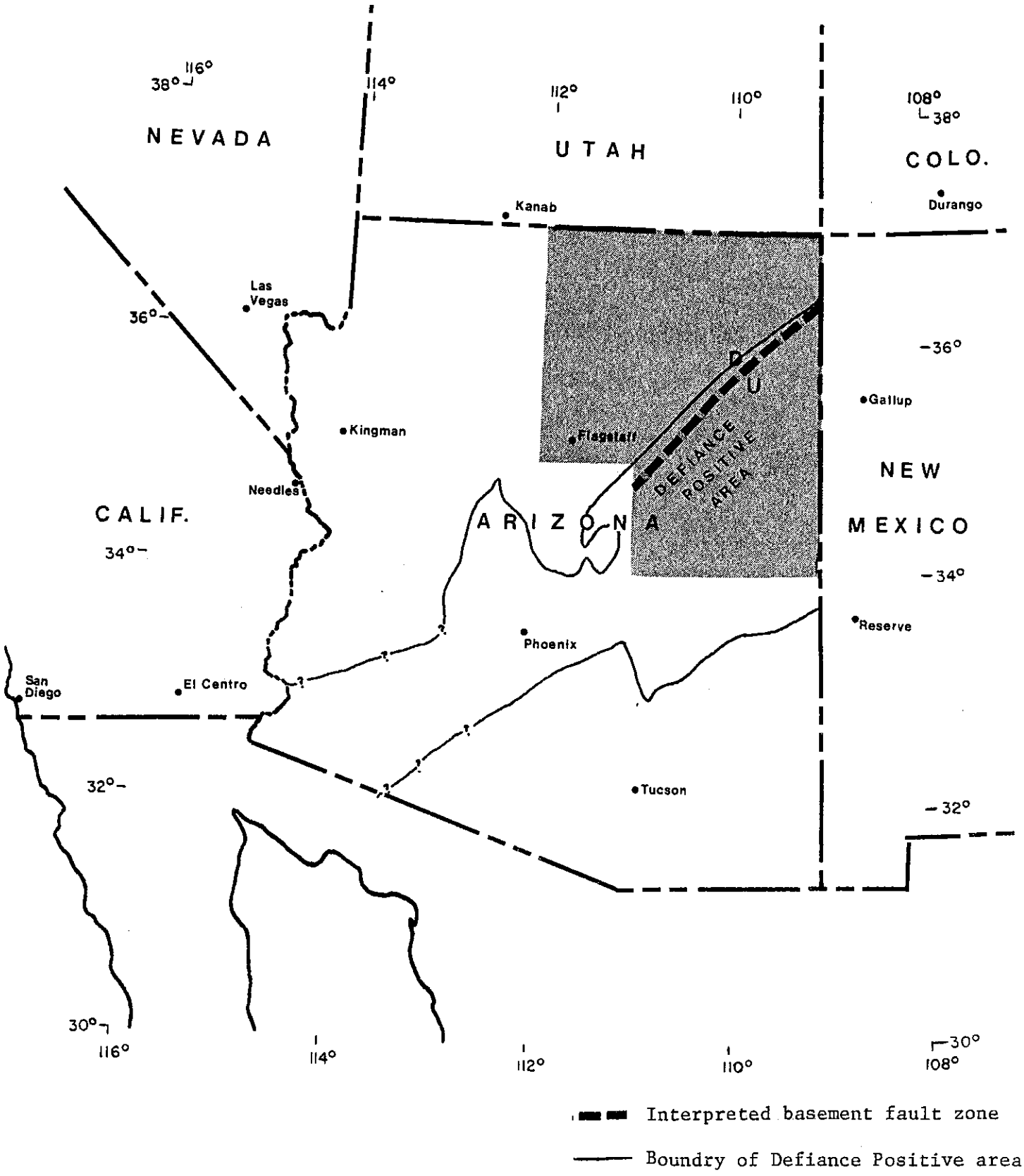

Fig. (15)

The Defiance Positive area and interpreted faulting in the Precambrian basement.

faults in the eastern portion of the area cut exposed Triassic and Jurassic sedimentary rocks. This fault may also be associated with a large southward swing in the course of the Little Colorado River near Winslow, Arizona, and northeast trending contacts between Tria-Jurassic and Tertiary sedimentary rocks further to the east.

8.1.3 Evidence for the Reactivation of Precambrian Faults During Cenozoic Time.

Walcott (1889) was presumably the first to identify the Precambrian origin for faults displacing Phenerizoic rocks of the Grand Canyon region. Wilson (1962) identifies a dominant trend of NE-SW for folds and faults of Precambrian origin in Arizona in contrast to the NW-SE and N-S trends associated with deformation of Laramide age and younger (contemporaneous with the Basin and Range Orogany).

Except in the western portion of the study area, the northeast trend is infrequently represented by surface geologic mapping (Plate 1). In contrast to this is the apparent profusion of interpreted faults, anomalous trends (especially in the gravity data (Plates 3 and 4)) and structural lineaments throughout the northern and western portions of

the study area. The spatial relationships between LANDSAT structural lineaments, interpreted faulting in the Precambrian basement and surficial geology suggest that these basement features may range from upper Paleozoic to Holocene age.

On LANDSAT scene 5667-16315 (Fig. 8) continuous and unbroken segments of the Additional Hill and Coconino Point monoclines trend northeast and northwest respectively. The continuity of these monocline segments suggests simultaneous movement along orthogonal faults, one of which clearly parallels the old Precambrian trend. It is interesting to note that this is not an isolated occurrence and that the observed continuity of trends (presumably "old" and "new) is well portrayed on this image.

8.2 Discussion of Implications to Regional Geology.

8.2.1 Transition from Basin and Range to Southern Colorado Plateau Provinces.

An examination of Plate 7 indicates that the style of deformation within the Colorado Plateau Province changes as one progresses northward from the Mogollon Rim. It appears that the so-called transition zone, defined from physiographic considerations, roughly corresponds to a zone of

transition from Basin and Range to Colorado Plateau style deformation. The southern portion of the study area, characterized by outcropping Precambrian igneous and metamorphic rocks, probably represents an exposed and highly eroded segment of the Precambrian basement which underlies the sedimentary rocks of the Plateau.

This observation suggests that the southern Colorado Plateau was probably subjected to the same forces that were responsible for the deformation of the Basin and Range Province. In support of this, it is noted that northeast trending structural lineaments interpreted from LANDSAT imagery of the White Mountain volcanic area (where rocks range from Quaternary to Holocene age) have essentially the same trend as interpreted faulting in the Precambrian basement somewhat further to the north.

8.2.2 The Structure of the Colorado Plateau.

Geophysical evidence from a variety of sources indicates that the crust of the Colorado Plateau is characterized by an anomalous thickness (35 kilometers), abnormally low P_n velocities (7.8 km/sec.) and is simultaneously in isostatic equilibrium (Woollard, 1972). These conditions require the Plateau to be topographically high and explain

the 1000 to 2000 foot elevation difference between it and the neighboring Basin and Range Province. In addition it is observed that a return to more normal P_n velocities and a decrease in crustal thickness occur toward the center of the Colorado Plateau, north of the Arizona - Utah border (Woollard, 1972).

It is suggested that the change in style (or reduction of intensity) of structures on the Colorado Plateau (with respect to the Basin and Range Province) are primarily the result of greater crustal competency and increased thickness. It is felt that the effect of this increase in crustal thickness is gradational, that the increase in thickness is roughly coincident with the high regional gravity gradient (Section 3.3.2, Figure 4) in the area, and accounts for the transitional style of deformation in the south (see Plate 7).

Examination of Figure 4, the regional Bouguer Anomaly map, indicates that in the western portion of the study area, the gravitational gradient maximizes approximately 40 to 50 kilometers northeast of the defined tectonic boundary of the Colorado Plateau (Fig. 2). It is hypothesized that this anomaly is caused by the gradual thickening of a low density crustal block (Fig. 16). This is undoubtedly a

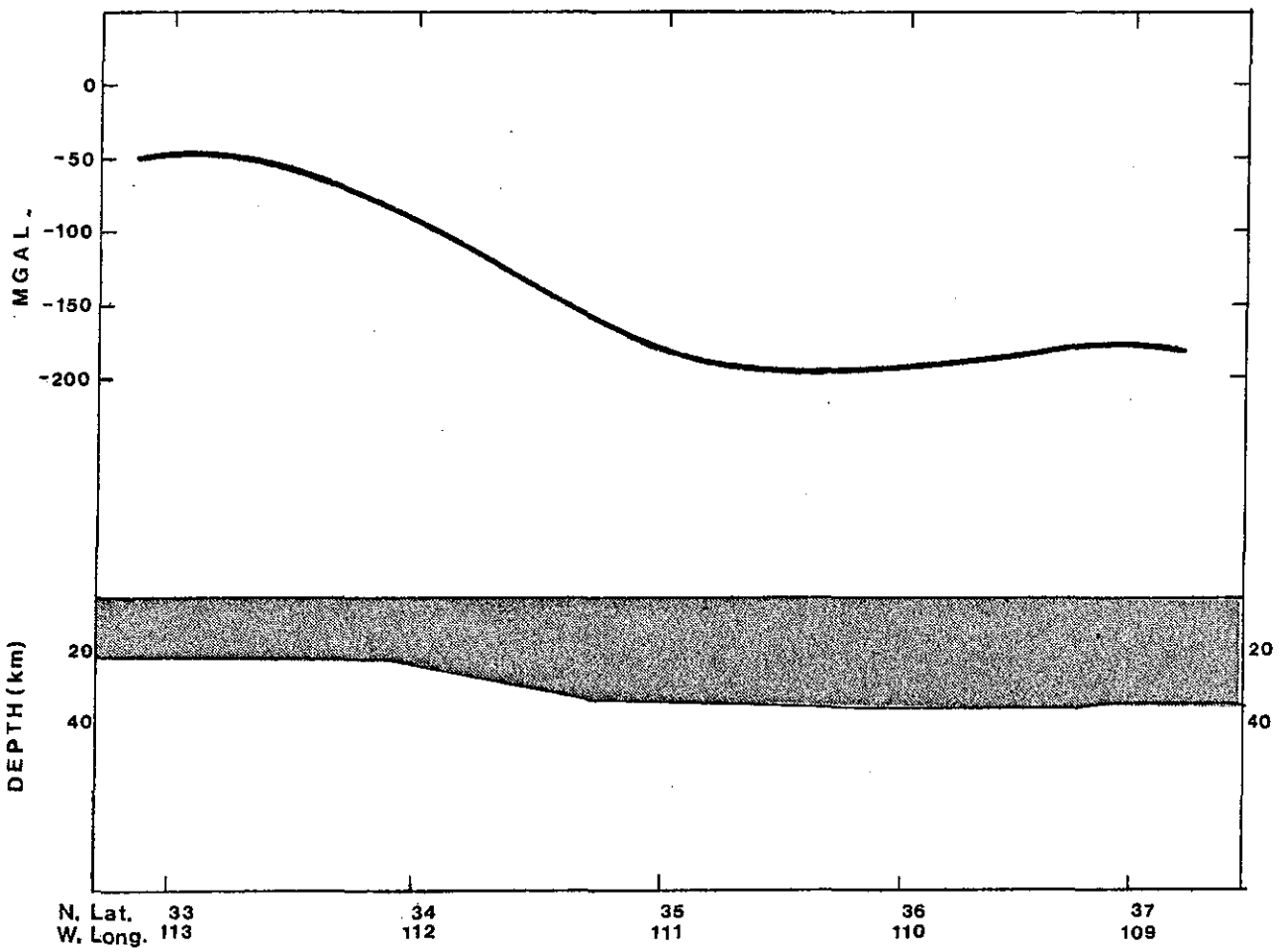

Fig. (16) Northeast-southwest profile across Northeastern Arizona study area illustrating the hypothetical relationship between Regional Bouguer gravity anomalies and crustal structure. Density contrast of model is 0.12 gm-cm^{-3}.

simplification of the actual condition at the southern Basin and Range - Colorado Plateau boundary, but it is probably sufficient to account for the observed anomaly pattern.

If it is further assumed that the Curie point isothermal surface roughly parallels, or is coincident with, the base of the block, (which hypothetically corresponds to the crust-mantle boundary) then essentially the same model described by Shuey (Shuey, et al, 1973) to explain magnetic anomalies associated with the Colorado Plateau - Basin Range boundary (400 kilometers to the north in Utah) has been described. It is noted that the offset of the edge of Shuey's model with respect to the defined tectonic boundary of the Plateau is approximately the same as described above. This suggests that the events which created the crustal thickening associated with the Colorado Plateau along its western boundary may also have been operational at its southern boundary. The differences in contemporary physiographic style in the two areas may be explained by their regional geologic environments and their tectono-structural histories.

8.3 Discussion of Implication to Economic Geology.

8.3.1 Oil and Gas Potential of Northeastern Arizona.

The totality of hydrocarbon and helium gas production in the State of Arizona occurs in the eastern third of the study area. Most of the production is from the Dinah-Bi-Keyah oil field which lies in the northwest end of the Toadlina Anticline. Production is from an igneous sill of Tertiary age that intrudes the Hermosa formation of Pennsylvanian age. This sill has apparently little or no geophysical expression at the scale of this study.

The relationship of the Dinah-Bi-Keyah field (as well as the other producing areas in northern Arizona, including the Bita Peak, Teek Nos Pos, Twin Falla Creek, East Boundary Butts and North Toh-Atin fields) with interpreted faulting and LANDSAT structural lineaments suggests that additional structural control may exist beyond the already defined controls.

An examination of Plates 1, 2 and 7 suggests several potentially interesting areas for hydrocarbon exploration. These include Red Rock Valley (37N-30E), Beautiful Valley (29N-9E), vicinity of St. Johns (15N-28E), Lyman Lake -

south of St. Johns (11N-28E), Limestone Ridge (9N-20E), vicinity of Holbrook (20N-20E), vicinity of the Comb Monocline in Cane Valley (41N-23E), and the Rankin and Paria Plateau in the extreme northeastern portion of the study area.

A shortcoming of northeastern Arizona with respect to its oil and gas potential is the apparent thinness of the sedimentary section. In the southern portion of the study area, the thickness of the sedimentary section is typically between 2000 and 4000 feet; it is only in the north that the section is observed to exceed 8000 feet, notably in the Black Mesa Basin and Cane Valley.

In the southern portion of the study area the lack of sedimentary section is somewhat compensated for by the presence of a thick and potentially petroliferous Permian section with several reported oil shows (the Supi Formation and the Coconino Sandstone, for example). The presence of numerous structural lineaments that correspond both spatially and in trend with interpreted faulting in the Precambrian basement suggests that these faults may cut the entire sedimentary section and provide, along with folding, additional traps for oil and gas. Northeast trending faults would, of course, be the most important. Potentially high geothermal gradients (which are assumed to have been present during the emplace-

ment of the volcanic rocks of the White Mountains and San Francisco Mountains may have helped to mature oil in the section and are considered a factor in favor of the oil and gas potential of the area.

8.3.2 Mineral Potential of Northeastern Arizona.

All of the major occurrences of economic mineralization in the study area were evaluated against the gravity, magnetic and LANDSAT data for any indications of possible relationships. Included in this check was an evaluation of geophysical anomaly characteristics (frequency, amplitude, etc.), spatial association with geophysical anomalies, spatial association with structural lineaments and tonal anomalies interpreted from LANDSAT imagery, and the intersections and aerial density of structural lineaments. No significant relationships were revealed and it is concluded that there are no immediate or apparent relationships between mineral occurrences and the geophysical data examined with these criteria at the scale of this study.

8.3.3 Geothermal Potential of Northeastern Arizona.

The presence of Tertiary to Holocene age volcanic rocks in the study area suggests that a geothermal energy

potential exists here. Of the three Cenozoic volcanic areas under evaluation, only the White Mountain and the San Francisco Mountains are deemed to have a significant potential from the standpoint of age and lithology.

The San Francisco volcanic area is currently under evaluation by scientists of the U. S. Geological Survey. The results of the gravity data presented in this study correlate quite well with data acquired and reduced independently by the USGS in Flagstaff, Arizona (Personal Communication, 1977).

Associated with the main body of the volcanic rocks are several residual gravity lows which could represent bodies within the crust with anomalous low densities. Because of the observed relationship between gravity lows, batholithic intrusions and molten magma chambers it is suggested that an evaluation of the areas encompassing these minima using other geophysical methods be performed. Methods such as intermediate-to-deep hole geothermal gradient and heat flow measurements, deep electromagnetic and electrical resistivity methods, and calculations of the depth to Curie Point isotherm using aeromagnetic data might provide useful information regarding the existence of viable geothermal resources and reservoirs.

The White Mountains of Arizona, it is believed, are largely unexplored and their geothermal potential is unknown. The existence of Tertiary and Holocene volcanic rocks of varying lithologies makes the area highly attractive from an exploration standpoint.

While the main body of the White Mountain volcanic area lies to the south of the study area, the northeast trending fault pattern (which is very apparent on the LANDSAT imagery to the south of the area) does appear in the interpreted basement fault pattern (Plate 7) further to the north. Analysis of magnetic data substantiates the results of field work and drilling which indicates that the volcanic cover in the study area is generally quite thin and is underlain by a substantial thickness of relatively non-magnetic sedimentary rock that may be heavily faulted. This could provide numerous exploration targets for geothermal resources.

APPENDICES

APPENDIX 1. DATA SOURCES FOR FIGURES AND PLATES

Figure	Title	Source(s)
1	Index map for southwestern United States showing location of U.S.G.C. Study Area	• U.S. Geological Survey 1:5,000,000 outline map
2	Tectonic Subdivisions of a portion of the Colorado Plateau	• Kelley Clinton, 1960 • Geologic Atlas of the Rocky Mountain Region, United States of America (1972) • Base: U.S. Geological Survey 1:2,500,000 base map
3	Seismicity map, showing epicentral locations for earthquakes, 1960-1974	• NOAA (1976) • Base: Same as Figure 2
4	Regional Bouguer Anomaly Map	• U.S. Air Force Aeronautical Chart and Information Center (1968) • Woollard and Joesting, Bouguer gravity anomaly map of the United States (1964) • West and Sumner, Bouguer Gravity anomaly map of Arizona (1973) • Base: Same as Figure 2
5	Regional Geothermal Gradient Map	• AAPG Geothermal Gradient map • U.S.G.S. Geothermal Gradient map of North America, 1977 • Base: Same as Figure 2
6	Index map showing locations of LANDSAT imagery used in Study	• U.S.G.S. EROS Data Center • Base: Same as Figure 1
7	LANDSAT image 2370-17233	• Base: U.S. Geological Survey 1:1,000,000 base map
8	LANDSAT image 5667-16315	• Base: Same as Figure 7
9	LANDSAT image 2367-17174	• Base: Same as Figure 7
10	LANDSAT image 2364-17181	• Base: Same as Figure 7
11	LANDSAT image 2369-17183	• Base: Same as Figure 7

Figure	Title	Source(s)
12	LANDSAT image 1210-17264	. Base: Same as Figure 7
13	LANDSAT image 5272-16512	. Base: Same as Figure 7
14	LANDSAT image 2350-17130	. Base: Same as Figure 7
15	Defiance Positive Area	. Base: Same as Figure 1 . Wilson (1962)
16	Crustal Configuration	. Figure 4

Plate	Title	Source(s)
1	Structural Elements of the USGS Study Area	. George Davis, Tectonic Analysis of Folds in the Colorado Plateau of Arizona, (1975). . Moore, Wilson, O'Haire, Geologic Map of Coconino County, Arizona (1960). . Moore, Wilson, O'Haire, Geologic Map of Navajo County, Arizona (1960). . Moore, Wilson, O'Haire, Geologic Map of Apache County, Arizona (1960). . Wilson, Moore, Geologic Map of Arizona (1969). . Base: USGS 1:500,000 State of Arizona (1972).
2	Structural Interpretation of LANDSAT Multispectral Imagery	. LANDSAT imagery, see Figures 7-14. . Base: same as Plate 1.
3	Observed Bouguer Gravity Anomaly Map	. Woollard and Joesting, Bouguer gravity anomaly map of the United States (1964). . West and Sumner, Bouguer gravity anomaly map of Arizona (1973). . Transcontinental Geophysical Survey (35^{o}-39^{o}N) Bouguer Gravity Map From 100^{o} to 112^{o}W Longitude (1968). . Base: same as Plate 1.

Plate	Title	Source(s)
4	Residual Bouguer Gravity Anomaly Map	. Same as Plate 3 and Figure 4. . Base: same as Plate 1.
5	Residual Magnetic Intensity Map	. Sauck and Sumner, University of Arizona Aeromagnetic Survey (1969). . Base: same as Plate 1.
6	Interpretation of Residual Bouguer Gravity	. Same as Plate 4. . Base: same as Plate 1.
7	Interpretation of Aeromagnetic Data	. Same as Plate 5. . Mitchell and Vargo, USGS Aeromagnetic Map of Hopi Buttes and Vicinity, Navajo County, Arizona (1966). . Frischknecht, Petrafesco, and others, USGS Aeromagnetic Map of Part of the Toh-Atin Mesa Quadrangle, Apache County, Arizona (1963). . Frischknecht, Petrafesco and others, USGS Aeromagnetic Map of the Canyon Del Muerto Quadrangle, Apache County, Arizona (1963). . Frischknecht, Petrafesco and others, USGS Aeromagnetic Map of the Nazline Quadrangle. Apache County, Arizona (1963). . Frischknecht, Petrafesco and others, USGS Aeromagnetic Map of Part of The Los Gigantes Buttes Quadrangle, Apache County, Arizona (1963). . Base: same as Plate 1.

APPENDIX 2. REGIONAL - RESIDUAL GRAVITY SEPARATION

The observed Bouguer Gravity data, Plate 3, and the Transcontinental Geophysical Survey data (USAF, 1968) was used to derive the regional and residual gravity maps shown in Figure 4 and Plate 4 respectively.

The regional gravity map was produced by the method of moving averages, which consists of smoothing the gravity map by replacing the value at each station with the average over a circle with a radius of 0.5 degrees. The regional can be written as

$$\bar{g}(r) = \frac{1}{2} \int_{\theta} g(r,\theta)\, d\theta \qquad \text{where,}$$

r = radius of the circle

$\bar{g}(r)$ = regional and

$g(r,\theta)$ = Bouguer gravity value at (r,θ) on the circumference of the circle.

Since values at discrete points are used, the integral is replaced by a sum and $\bar{g}(r)$ is calculated numerically as

$$\bar{g}(r) = \sum_{i=1}^{h} g(r,\theta_i)/n$$

The residual gravity map was then produced by gridding the regional gravity and subtracting it point by point from the gridded observed Bouguer anomaly values.

APPENDIX 3. CONTINUATION OF AEROMAGNETIC DATA

The data used to produce the residual aeromagnetic map, Plate 5, was flown at two altitudes. The flight lines from longitude 112° to approximately 110° were flown at 9,000 feet, and those from longitude 110° to the eastern Arizona border were flown at 11,000 feet. The values east of longitude 110° were downward continued 2,000 feet. The method used (Lourenco, 1972) is based on the two-dimensional Fourier transform of the residual aeromagnetic data.

The residual field values, $T(X, Y, O)$ are represented on a grid as T_{jk}, where

$$T_{jk} = T(js, ks)$$

$j = O, 1, \ldots, M-1$

$k = O, 1, \ldots N-1$ and S is the grid spacing

M = number of samples along X axis

N = number of samples along Y axis

From T_{jk}, the double Fourier transform,

$$W_{T_{mn}} = \frac{1}{MN} \sum_{j=0}^{M-1} \sum_{k=0}^{N-1} T_{jk} \cdot \exp\left(-2\pi i\left(\frac{jm}{M} + \frac{kn}{N}\right)\right)$$

is calculated using the fast Fourier transform (Cooley and Tuckey, 1965). From $W_{T_{mn}}$ the three components of the field, Hx, Hy and Hz, can be calculated using the finite harmonic expansion,

$$\begin{bmatrix} Hx \\ Hy \\ Hz \end{bmatrix} = \sum_{n=-N/2}^{N/2} \sum_{M=-M/2}^{M/2} \begin{bmatrix} W_{X_{mn}} \\ W_{Y_{mn}} \\ W_{Z_{mn}} \end{bmatrix} \cdot \exp\left(2\pi \left(\frac{m^2}{x^2} + \frac{n^2}{y^2} \right)^{1/2} z \right)$$

$$\cdot \exp\left(2\pi i \left(\frac{mx}{x} + \frac{ny}{Y} \right) \right)$$

where $x = M_s$

$y = N_s$

Hx = horizontal component (northward)

Hy = transverse component (eastward)

Hz = vertical component (downward)

and $W_{X_{mn}}$, $W_{Y_{mn}}$ and $W_{Z_{mn}}$ are the discrete Fourier coefficients for Hx, Hy and Hz respectively. The three components Hx, Hy and Hz are now calculated at any level z above or below the measurement plane, z = 0, using the above harmonic series. The residual field at level z is then calculated by

$$T(X, Y, Z) = \alpha H_x(X, Y, Z) + \beta H_y(X, Y, Z) + \gamma H_z(X, Y, Z)$$ where

α, β and γ are the direction cosines of the earth's geomagnetic field over the area.

APPENDIX 4. GRIDDING AND CONTOURING

The gridding and contouring routines used to produce the gravity and magnetic maps included in this report are proprietary. The gridding program calculates a rectangular array of data points from randomly spaced points. The surface produced by this program approaches the smoothest surface passing through all the data points by following the principle of minimum total curvature. This principle yields surfaces which are smooth where data is sparse and detailed where data is dense.

The contouring package assumes the surface varies smoothly between contour levels and uses linear interpolation to produce values needed for contouring.

APPENDIX 5. DEPTH TO MAGNETIC BASEMENT CALCULATIONS

The data used to create the aeromagnetic map of the area (Plate 5) was used to calculate the depths to magnetic basement. Well data was used wherever available for control.

The method used to calculate the depths consists of resolving anomalies due to two dimensional structures (Nabighian, 1972 and Hartman, et at, 1971). A profile is selected which corresponds to a flight line. The Fourier transform and horizontal derivative of the total field along this line are calculated. A new spectrum is defined by transforming the Fourier series as follows,

$$\overline{F}(W) = \begin{cases} 2F(W) & \text{for } W > 0 \\ F(W) & \text{for } W = 0 \\ 0 & \text{for } W < 0 \end{cases}$$

where F(W) is the Fourier transform of the total field or horizontal derivative. The inverse Fourier transform of $\overline{F}(W)$ is calculated and the amplitude square, a(x), curve is plotted. The a(x) curve represents a superposition of symmetric and antisymmetric curves. The symmetric portion of the a(x) curve is a combination of bell-shaped curves each being situated over the top of thin sheets or prisms with their half-maximum half-width equal to the depth to the top of the body. In order to resolve a(x) into symmetric and antisymmetric curves it is necessary to identify the number and location of bell-shaped curves. The location and number of curves are determined by using the Werner Deconvolution.

The Werner Deconvolution resolves anomalies due to two dimensional structures and consists of solving a set of (n + 5) equations for (n + 5) unknowns, where

$$F(X_i) = \frac{A(x_i - x_o) + z}{(x_i - x_o)^2 + z^2} + C_o + C_1 X_i + \ldots + C_n X_i^n$$

and $i = 1, 2, \ldots, n + 5$

$F(X_i)$ = total field or horizontal derivative at point X_i along the profile,

X_o = horizontal location of the edge of a thin sheet,

Z = depth to the edge of the sheet,

and A, B, C_o, C_1, $\ldots$, C_n are constants. Solving this set of equations along the profile for each set of (n + 5) consecutive points yields a scatter of X_o locations concentrating around the edges of the sheets. Once the edge locations are determined, the symmetric function corresponding to each edge is used to determine the depth to the top of the sheet or prism.

REFERENCES CITED

Agarwal, R. G. and Kanasewich, E. R., Automatic Trend Analysis and Interpretation of Potential Field Data, Geophysics, v. 36, no. 2, p. 339-348, 1971.

Algermissen, S. T., and Perkins, D. M., A Technique for Seismic Zoning: General Consideration and Parameters, in International Conference on Microzonation for Safer Construction, Research and Applications, Proceedings, v. 2; University of Washington, Seattle, p. 865-878, 1972.

American Association of Petroleum Geologists, Geothermal Survey of North America Portfolio Gradient Maps (18 and 19).

Arizona State Oil and Gas Conservation Commission, Subsurface Temperature Map, 1972.

Baker, A. A., Geologic Structure of Southeastern Utah, in, Am. Assoc. Pet. Geol. Bull., v. 19, p. 107-150, 1955.

Barwin, John R., King, Robert W., and Hassenfratz, Charles A., Future Oil and Gas Potential of Northeastern Arizona, AAPG Journal, 1969.

Brown, S. C., and Lauth, R. E., Oil and Gas Potentialities of Northern Arizona, in Guidebook of the Black Mesa Basin, Northeastern Arizona, N. Mex. Geol. Soc. 9th Field Conf., p. 153-160, 1958.

Case, J. E. and Joesting, H. R., Regional Geophysical Investigations in the Central Colorado Plateau, Geological Survey Professional Paper 736, 1973.

Cooley, J. W., and Tukey, J. W., An Algorithm for the Machine Calculation of Complex Fourier Series: Math. of Computation, v. 19, no. 90, p. 297-301, 1965.

Davis, G. H., Tectonic Analysis of Folds in the Colorado Plateau of Arizona, Office of Arid Lands Studies Bulletin 9, Univ. of Arizona, p. 68, 1975.

Drake, C. L., and Nafe, J. E., The Transition from Ocean to Continent from Seismic Refraction Data, in The Crust and Upper Mantle of the Pacific Area, Am. Geophys. Union Geophys. Monograph 12, L. Knopoff, C. L. Drake and P. J. Hart, ed., p. 174-186, 1968.

Gilluly, J., Tectonics Involved in the Evolution of Mountain Ranges, in The Nature of the Solid Earth, Robertson, E. C., ed., McGraw Hill International Series in the Earth and Planetary Sciences, p. 406-439. 1972.

Goetz, A. F., Billingsley, F. C., Gillespie, A. R., Abrams, M. J., Squires, R. L., Shoemaker, E. M., Lucchitta, I. and Elston, D. P., Application of ERTS Images and Image Processing to Regional Geologic Problems and Geologic Mapping in Northern ARizona, Jet Propulsion Laboratory Technical Publication 32-1597, California Institute of Technology, 1975.

Hartman. Ronald R., Teskey, Dennis J., and Friedberg, Jeffrey L., A System for Rapid Digital Aeromagnetic Interpretation, Geophysics, v. 36, no. 3, p. 891-918, 1971.

Hodgson, R. A., Genetic and Geometric Relations Between Structures in Basement and Overlying Sedimentary Rocks with Examples from Colorado Plateau and Wyoming, in Am. Assoc. Petroleum Geologists Bull., v. 49, p. 935-949, 1965.

_____, Regional Study of Jointing in Comb Ridge - Navajo Mountain Area, Arizona and Utah, in Am. Assoc. Petroleum Geologists Bull., v. 45, p. 1, 38, 1961.

Kaula, W. M., A Tectonic Classification of the Main Features of the Earth's Gravitational Field, J. Geophys. Res., 74, p. 4807-4826, 1969.

Kelley, V. C. Tectonics of the Black Mesa Basin of Arizona, in Guidebook of the Block Mesa Basin, Northeasthern Arizona, N. Mex. Geol. Soc. 9th Field Conf., p. 137-144, 1958.

Kelley, V. C., and Clinton, N. J., Fracture Systems and Tectonic Elements of the Colorado Plateau, Univ. of N. Mex. Pubs. in Geol., No. 6, p. 104, 1960.

_____, Monoclines of the Colorado Plateau, in Geol. Soc. America Bull., v. 66, p. 789-804, 1955a.

_____, Regional Tectonics of the Colorado Plateau and Relationship to the Origin and Distribution of Uranium, Univ. of N. Nex. Pubs. in Geol., no. 5, p. 120, 1955b.

Ligett, M. A., and Research Staff, A. Reconnaissance Space Sensing Investigation of Crustal Structure for a Strip from the Eastern Sierra Nevada to the Colorado Plateau: Argus Exploration Company, NASA Final Report Inv., NASA-CR-139434, E74-10705, 1974.

Lourenco, Jose Seixas, Analysis of Three-Component Magnetic Data, Ph. D. Dissertation, University of California, Berkley, 1972.

Mathews, V., and Anderson, C. E., Yellowstone Convection Plume and Break-up of the Western United States, Nature, v. 243, p. 158-159, 1973.

Nabighian, Misac N., The Analytic Signal of Two Dimensional Magnetic Bodies With Polygonal Cross-Section: Its Properties and Use For Automated Anomaly Interpretation; Geophysics, v. 37, no. 3, p. 507-617, 1972.

National Oceanic and Atmospheric Administration, National Geophysical and Solar-Terrestrial Data Center, Boulder, Colorado, 1976.

Roy, R. F., Decker, E. R., Blackwell, D. D., and Birch, F., Heat Flow in the United States, J. Geophys. Res., v. 73, p. 5207-5221, 1968.

Roy, R. F., Blackwell, D. D., and Decker, E. R., Continental Heat Flow, in The Nature of the Solid Earth, etc. ..., p. 506-543, 1972.

Sauck, W. A., and Sumner, J. S., Aeromagnetic Survey of Arizona, Total Magnetic Intensity with the International Geomagnetic Reference Field (IGRF), epoch 1965, removed, Laboratory of Geophysics of the University of Arizona, 1970.

Shuey, R. T., Schellinger, D. K., Johnson, E. H., and Alley, L. B., Aeromagnetics and the Transition Between the Colorado Plateau and Basin Range Provinces, Geology, v. 1, p. 107-110, 1973.

Simon, R. B., "Seismicity," in Geologic Atlas of the Rocky Mountain Region, United States of America, Rocky Mountain Association of Geologists, p. 48-51, 1972.

Smiley, T. L., The Geology and Dating of Sunset Crater, Flagstaff, Arizona, in Guidebook of the Black Mesa Basin - Northeastern Arizona, New Mexico Geological Society, p. 186-190, 1958.

Smith, R. B., and Sbar, M. L., Contemporary Tectonics and Seismicity of the Western United States with Emphasis on the Intermountain Seismic Belt, Geological Society of America Bulletin, v. 85, p. 1205-1218, 1974.

United States Air Force Aeronautical Chart and Information Center, Transcontinental Geophysical Survey (35°-39°N), Bouguer Gravity Map from 100° to 112°W Longitude, U. S. Geological Survey Map I-533-B, 1968.

U. S. Geological Survey and American Association of Petroleum Geologists, Tectonic Map of the United States, 1961.

Walcott, C. P., Study of a Line of Displacement in the Grand Canyon of the Colorado, in Northern Arizona, U. S. Geological Survey Bull., v. I, p. 49-64, 1889.

Warren, D. H., Transcontinental Geophysical Survey (35^{o}-39^{o}N), Seismic Refraction Profiles of the Crust and Upper Mantle from 100^{o} to 112^{o}W Longitude, U. S. Geological Survey Map I-533-D, 1968.

Warren, R. E., Sclater, J. G., Vacquier, V., and Roy, R. F., A Comparison of Terrestrial Heat Flow and Transient Geomagnetic Fluctuations in the Southwestern United States, in Geophysics, v. 34, p. 463-478, 1969.

West, R. E., and Sumner, J. S., Bouguer Gravity Anomaly Map of Arizona, Laboratory of Geophysics of the University of Arizona, 1973.

Wilson, Edred D., and Moore, Richard T.; Geologic Map of Arizona, Arizona Bureau of Mines and United States Geological Survey; 1969.

Wilson, E. D., A Resume of the Geology of Arizona, Arizona Bureau of Mines Bull., v. 171, p. 140, 1962.

Woodward, L. A., Structural Framework and Tectonic Evolution of the Four Corners Region of the Colorado Plateau in Guidebook of Monument Valley and Vicinity, Arizona and Utah, N. Mex. Geol. Soc. 24th Field Conf., p. 94-98, 1973.

Woollard, G. P., A Regional Analysis of Crustal Structure in North America, United States Air Force, Aeronautical Chart and Information Center, HIG-69-12, 1969.

Woollard, G. P., and Joesting, H. R., Bouguer Gravity Anomaly Map of the United States (exclusive of Akaka and Hawaii), American Geophysical Union, Special Committee for the Geophysical and Geological Study of the Continents, U. S. Geological Survey Spec. Map, 2 sheets, 1964.

Woollard, G. P., Regional Variations in Gravity, in The Nature of the Solid Earth, Robertson, E. D., ed., McGraw Hill International Series in the Earth and Planetary Sciences, p. 463-505, 1972.